frontiers | Frontiers in Earth Science

ORIGINAL RESEARCH
published: 13 July 2022
doi: 10.3389/feart.2022.834029

Coexistence of Adjacent Siliciclastic, Carbonate, and Mixed Sedimentary Systems: An Example From Seafloor Morphology in the Northern Lesser Antilles Forearc

Pierre Morena[1,2], Gueorgui Ratzov[2], Antonio Cattaneo[1], Frauke Klingelhoefer[1], Christian Beck[3], Chloé Seibert[4], Boris Marcaillou[2] and Nathalie Feuillet[4]*

[1]Geo-Ocean, Univ Brest, CNRS, Brest, France, [2]Université Côte d'Azur, CNRS, IRD, Observatoire de la Côte d'Azur, Géoazur, Valbonne, France, [3]CNRS ISTerre, Université Savoie-Mont-Blanc, Le Bourget du Lac, France, [4]Institut de Physique du Globe de Paris, CNRS, Université de Paris-Cité, Paris, France

OPEN ACCESS

Edited by:
Adam McArthur, University of Leeds, United Kingdom

Reviewed by:
Barbara Claussmann, Schlumberger, United Kingdom
Lesli Wood, Colorado School of Mines, United States

***Correspondence:**
Pierre Morena
pierre.f.morena@gmail.com

Specialty section:
This article was submitted to Sedimentology, Stratigraphy and Diagenesis, a section of the journal Frontiers in Earth Science

Received: *12 December 2021*
Accepted: *07 June 2022*
Published: *13 July 2022*

Citation:
Morena P, Ratzov G, Cattaneo A, Klingelhoefer F, Beck C, Seibert C, Marcaillou B and Feuillet N (2022) Coexistence of Adjacent Siliciclastic, Carbonate, and Mixed Sedimentary Systems: An Example From Seafloor Morphology in the Northern Lesser Antilles Forearc. Front. Earth Sci. 10:834029. doi: 10.3389/feart.2022.834029

Three main types of factors commonly control the nature of the clasts, the arrangement of the distinctive lithologies, and the general architecture of turbidite systems: sedimentation rate and carbonate production; climates and glacio-eustatism; and morphology and tectonics. The coexistence of adjacent systems of distinctive nature is, however, scarcely documented, and the relative influence of each factor needs better constrain. In the Northern Lesser Antilles Segment (NLAS), carbonate and siliciclastic sediment sources coexist within a 150 km lateral distance, with carbonate platforms lying onto a volcanic substratum, and by a succession of spurs and triangular valleys that are bounded by active normal faulting. To better understand the factors controlling sedimentary processes from the carbonate platform sources to the deep-sea sinks, we used backscatter, bathymetry, multichannel seismic, and sub-bottom profiles. Sedimentary systems are dominated by siliciclastic input (by retrogressive erosion of confined canyons affecting the volcanic slope), carbonate input (by carbonate sediment transported by oceanic- and wind-driven submarine currents beyond the leeward edges of carbonates platforms), or both. In the mixed systems, the retrogressive erosion of the canyon head determines the nature of the source (volcanic on the slope, carbonate when the canyons reach the shelf edge). Glacio-eustatism has a key role in carbonate availability on the platform, as attested by the presence of drowned platforms. The main contribution of this study is the identification of the major role that tectonic activity plays in the short-distance coexistence of the distinctive sedimentary systems since fault-bounded V-shaped valleys in map view offer alternating leeward and windward edges favoring carbonate or mixed systems. Additionally, the steep slope gradient induced by normal faults and regional subsidence seems to be the main factor controlling sediment dispersal. It causes multiple line sources and the dispersion of gravity-driven currents under the effect of hydraulic jumps, thus preventing the formation of a channelized system. Our study provides a modern analog of adjacent systems dominated by distinctive lithologies in a tectonically active area. The results appear particularly appropriate to decipher the nature of ancient

source-to-sink systems dominated by complex tectonics, paleo-bathymetry, and sediment routings.

Keywords: sediment pathways, mixed turbidite system, subduction zone, submarine canyon, plunge-pool, active tectonics

1 INTRODUCTION

The identification of the main depositional elements in sedimentary systems, especially for the lowest part of the systems where gravity flows and turbidity currents dominate, was proposed first in siliciclastic systems, in particular concerning the architecture of turbidite systems that include sediment sources on land and on the shelf, canyons on the continental slope, channel-levee systems, and distal fan systems in the abyssal plain (Mutti and Normark, 1991; Shanmugam, 2016). Gravity flows typically funneled into point sources constitute a morphological control leading to such architecture (Yose and Heller, 1989 and references therein). Differences in sedimentary systems, such as morphology and timing of clastic production, do exist. Indeed, carbonate gravity flows are commonly triggered from a line of sources at the shelf edge or along the slope (Mullins et al., 1984; Droxler and Schlager, 1985; Reijmer et al., 1988; Haak and Schlager, 1989; Mulder et al., 2012b), diluting the amount of sediment, thus deep water carbonates systems are considered to lack well-developed channel-levee and lobe deposits (Yose and Heller, 1989). The timing of sediment transfer may also differ, with carbonate systems being more productive during sea-level high stands (Reijmer et al., 1988), while pure siliciclastic systems are more active during relative sea-level low stands (Posamentier et al., 1991; Vail et al., 1991; Hübscher et al., 1997). Likewise, in the mixed systems, the dominance of the carbonate sources during sea-level highstands/warm periods and dominance of the siliciclastic sources during sea-level low stands/cool periods are generally observed (Schlager et al., 1994; Jorry et al., 2008). The "dominant" system usually restrains the other system (e.g., carbonate reefs prevent the siliciclastic input, Puga-Bernabéu et al., 2011; 2014; Moscardelli et al., 2019).

Over the two last decades, a series of studies conducted in ancient (Dorsey and Kidwell, 1999; Braga et al., 2001; Payros and Pujalte, 2008; Sola et al., 2017; Chiarella et al., 2017; 2019) and modern depositional systems (Mulder et al., 2012a; 2012b; Principaud et al., 2015; Tournadour et al., 2015, 2017; Counts et al., 2018; Jorry et al., 2020) reveal multiple examples with similar morphologies and architectural elements between siliciclastic, carbonate, and mixed turbidite systems. To predict the nature of the clasts, the arrangement of the distinctive types of deposits, and the general architecture of the turbidite systems, the authors emphasize the influence of three main types of factors. These include first, the sedimentation rate and carbonate production (Dorsey and Kidwell, 1999; Jorry et al., 2008; Counts et al., 2018; Jorry et al., 2020); second, climate, and eustatism (Spence and Tucker, 1997; McArthur et al., 2013; Puga-Bernabéu et al., 2014; Cumberpatch et al., 2021); third, the morphology and tectonic displacements of the source areas (Bailleul et al., 2007; Reijmer et al., 2012; Ćosović et al., 2018; Claussmann et al., 2021a; Claussmann et al., 2021b). The coexistence of adjacent systems of distinctive nature is however scarcely documented, and the relative influence of each factor needs to be better constrained.

In this study, we propose a detailed morphological analysis of a marine dataset from the Northern Antilles area, and in particular from the Northern Lesser Antilles Segment (NLAS). This area extends from the inactive volcanic arc to the subduction front between Antigua and Anguilla banks (**Figure 1**). The NLAS is composed of carbonate shelves resting on a volcanic basement where structural features control the overall morphology of the margin (Feuillet et al., 2002; Laurencin et al., 2017; Boucard et al., 2021), and the connectivity of carbonate reefs to the deeper part of turbiditic sedimentary systems. The coexistence of adjacent siliciclastic, carbonate or mixed sedimentary systems make the NLAS an ideal case to identify the mechanisms and controls of sediment distribution from the carbonate shelf sources to deep-sea sinks in the forearc. We anticipate the application of this case in both modern and ancient systems dominated by tectonics and presenting complex morphologies, sediment pathways, and sediment accumulation. We present new backscatter and bathymetric data, multichannel seismic profiles (MCS profiles), and sub-bottom profile data (**Figure 2**) to: 1) identify the sediment sources and pathways of gravity-driven currents and sediment transfer, from the carbonate shelf down to the slope in the forearc zone of the NLAS, 2) identify the signature of dominant processes that influence sediment remobilization and transfer, and 3) infer their variability over time.

2 GEOLOGICAL SETTING

2.1 Geodynamics of the Lesser Antilles

The Lesser Antilles Volcanic Arc results from the subduction of the upper Cretaceous (~100 Ma) oceanic lithosphere (Stein et al., 1982; Stéphan et al., 1990), part of the North and South American plates, beneath the Caribbean plate (**Figure 1A**). The present-day convergence rate is ~20 mm/year along a ~N254° direction (De Mets et al., 2010).

The primary arc of the Lesser Antilles was formed during the Eocene to the early or the middle Miocene (Bouysse and Guennoc, 1983; Legendre et al., 2018). It comprises volcanic islands from Dog Island to Guadeloupe and from St. Lucia to Grenade (**Figure 1**). Tectonic uplift was responsible for the emergence of some carbonate platforms such as Marie-Galante, Barbuda, and Anguilla (Budd et al., 1995; Feuillet et al., 2004; Cornée et al., 2012:; Weil-Accardo et al., 2022). The uplift results either from backarc spreading in the Kalinago Basin (**Figures 1B,C**) during the earliest-middle Miocene (Boucard et al., 2021) or from long-term processes along the subduction megathrust during the Pliocene (Feuillet et al., 2004; Leclerc and Feuillet, 2019).

The subduction of Tiburón ridge (**Figure 1**) during the middle to the late Miocene (Pichot et al., 2012) and Barracuda ridge

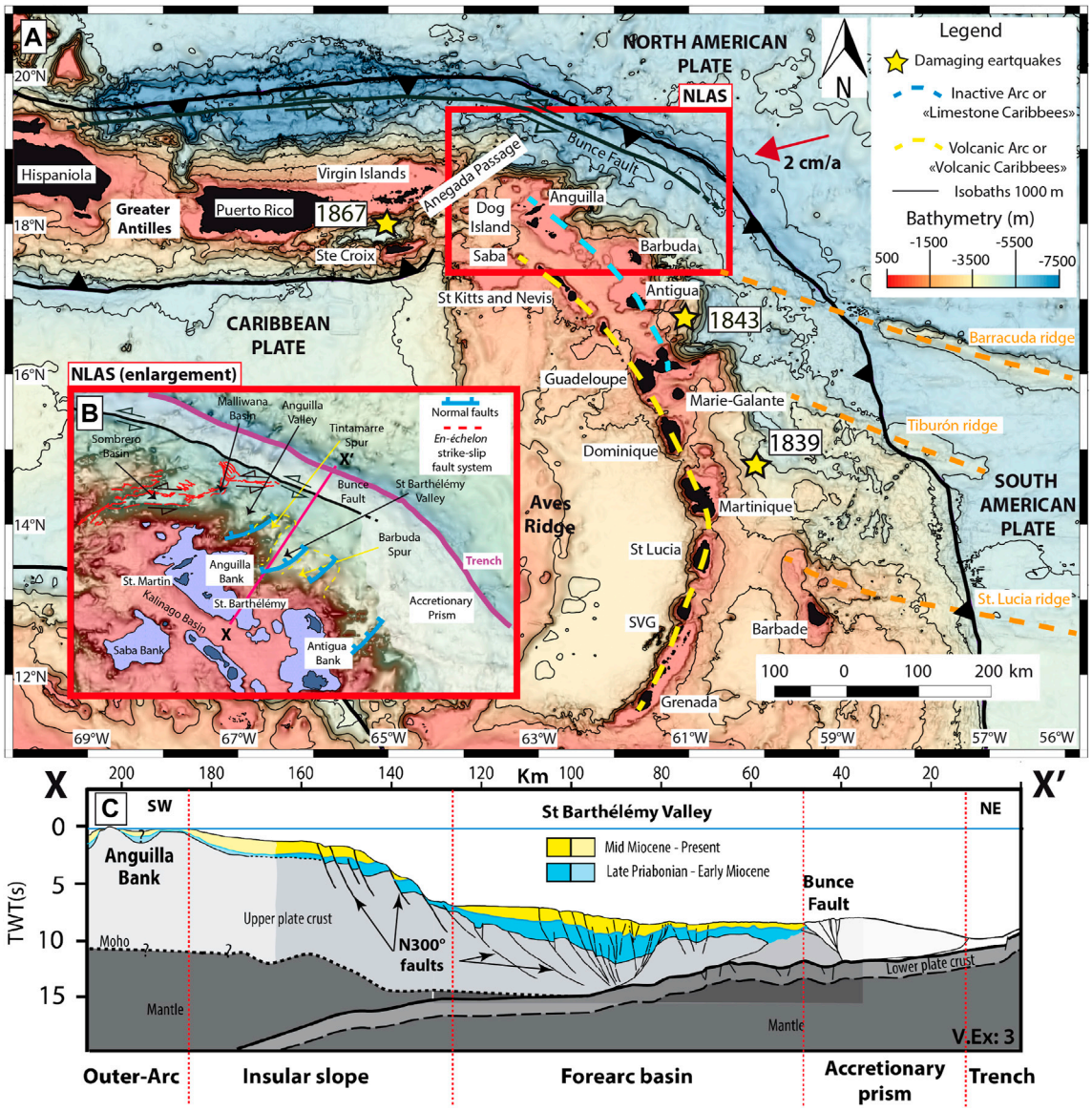

FIGURE 1 | (A) General map of the Lesser Antilles subduction zone. The red box indicates the study area (the NLAS) and refers to **Figure 1B** and **Figure 2**. The orange dashed lines represent the ridges. **(B)** Enlargement of the Northern Lesser Antilles Segment. **(C)** XX′ cross-section (modified from Boucard et al., 2021).

(**Figure 1**) during the Pleistocene (Pichot et al., 2012) may have caused a slight transverse shift of the volcanic front (Bouysse and Westercamp, 1990) and resulted in a morphological segmentation of the forearc. The subduction of these ridges may have in addition promoted a change in the dip of the subducting slab (Bouysse and Westercamp, 1990). Consequently, the volcanism migrated southwestward and formed, during the late Miocene (Bouysse and Westercamp, 1990), the islands of the inner, secondary and active arc called "Volcanic Caribbees", which include islands from Saba to Grenada (**Figure 1**). The northward increasing obliquity of the subduction (from 16° east of Guadeloupe to 75° northeast of the Virgin Islands) is partially accommodated by sinistral strike-slip deformation along the "Volcanic Caribbees" (Feuillet et al., 2002; Feuillet et al., 2004; Feuillet et al., 2010; Feuillet et al., 2011), in the Anegada Passage (Laurencin et al., 2017), and by strike-slip faults in the accretionary prism (Laurencin et al., 2019, or; Benâtre et al., 2020).

2.2 The Northern Lesser Antilles Segment (NLAS)

The NLAS is limited to the northwest by the Anegada Passage (Jany et al., 1990), which separates the Lesser Antilles to the east from the Greater Antilles to the west (Christman, 1953). The Anegada Passage extends eastward to the accretionary prism through a continuous set of *en-échelon* strike-slip faults (**Figure 1B**) and pull-apart basins (Sombrero, Malliwana,

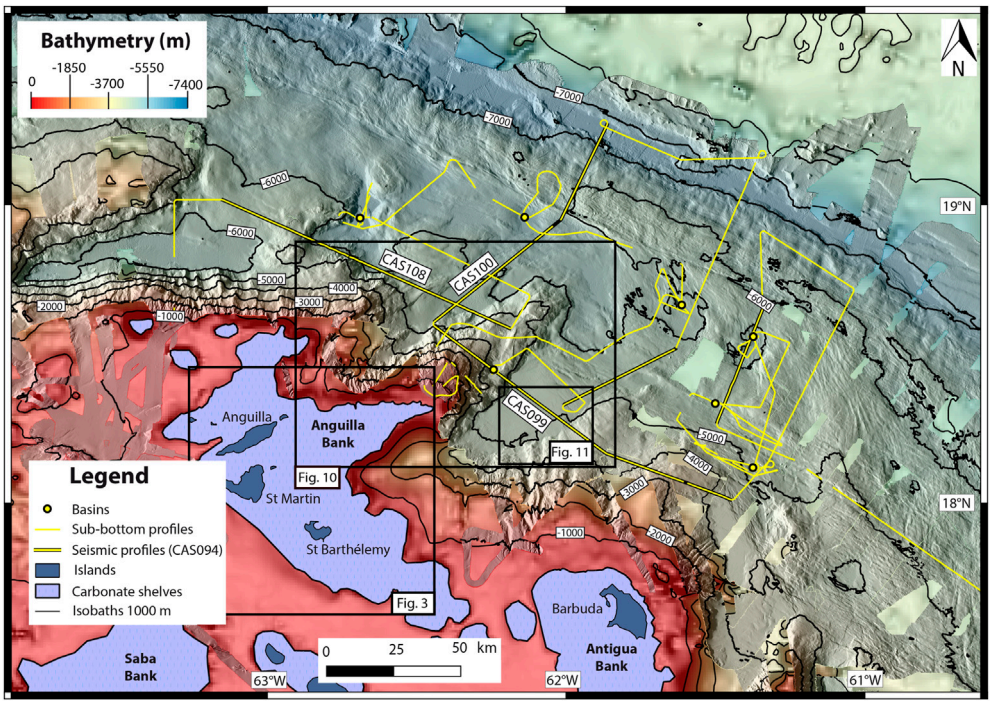

FIGURE 2 | Data from ANTITHESIS (2013–2016) and CASEIS (2016) cruises in the NLAS. Black lines represent the seismic profiles: CAS108 (**Figures 7A**, **10**), CAS099 (**Figure 7B**), and CAS100 (**Figure 10**). Black boxes locate **Figures 3**, **10**, **12**.

Figure 1B) called the Anegada Passage Eastern Segment (Laurencin et al., 2017). At its eastern limit, the passage connects to the sinistral strike-slip Bunce Fault (**Figure 1B**) that extends from Puerto Rico (ten Brink et al., 2004) to offshore Barbuda (Laurencin et al., 2019). To the west, the 800-m-deep Kalinago Basin (**Figures 1B,D**; Legendre et al., 2018), which opened as an intra-arc basin during the late Eocene-early Oligocene (Cornee et al., 2021), separates the NLAS from the inner and active arc (**Figure 1A**; Bouysse et al., 1985; Jany et al., 1990).

In the NLAS, the Eocene to Miocene volcanic basement is overlain by shallow Miocene to Holocene carbonate platforms such as the Antigua Bank or the Anguilla Bank (**Figures 1B**, **2**, **3**). These banks include a few islands (Antigua and Barbuda on the Antigua Bank and Anguilla, St. Barthélémy and St. Martin for the Anguilla Bank; **Figure 1**) that were probably connected during the Pliocene and the Pleistocene when the sea-level was lower (Christman, 1953; Cornee et al., 2021). The volcanic basement outcrops in the islands of the Anguilla Bank, where it was tilted by NE-SW faults (Cornee et al., 2021). It consists of late Paleocene to Eocene volcaniclastic turbidites (Andréïeff et al., 1988a; Andréïeff et al., 1988b), late Eocene-early Oligocene intruded granodiorites (Nagle et al., 1976), and Oligocene to early Miocene volcanic pipes and intrusions (Nagle et al., 1976). On the Antigua Bank, volcanic rocks are only observed in Antigua Island and consist of a middle Eocene to Oligocene basal volcanic complex (Briden et al., 1979) and Oligocene volcaniclastic deposits (Mascle and Westercamp, 1983).

The seafloor morphology presents a steep insular slope (Bouysse and Guennoc, 1983; **Figures 1B,C**) and a succession of arc-perpendicular spurs (Barbuda, Tintamarre, **Figure 1B**) and V-shaped valleys in map view (Anguilla, St-Barthélémy;) bounded by NE-SW (N40°–90°) normal faults in the forearc (Feuillet et al., 2002; Boucard et al., 2021). The N40°–90° normal faults and the strike-slip faults of the Anegada Passage Eastern Segment either accommodated since the late Paleogene (Pindell and Kennan, 2009) the Bahamas Bank collision, and the subsequent margin convex bending (Pindell and Barett, 1990; Mann et al., 2005; Boucard et al., 2021) or plate-scale slip-partitioning (Feuillet et al., 2002; Feuillet et al., 2004; Feuillet et al., 2010; Feuillet et al., 2011). The V-shaped valleys opened during a trench-parallel extension phase that triggered crustal normal faulting before the earliest middle Miocene when an emersion phase occurred (Boucard et al., 2021). Additionally, the margin is cut by a series of ~N300° trending normal faults (**Figure 1B**) generated during a trench-perpendicular extension, and associated with post-Miocene drastic subsidence (estimated about 340 m/Myr since 16 Ma, Boucard et al., 2021), a Pliocene to Present basal erosion of the upper plate and a major basement thinning (Boucard et al., 2021). The NLAS is similar to the "Rough area" defined by Seibert et al. (2020) north of the Désirade normal fault comprising wide carbonate platforms, straight canyons incising a steep insular slope, and deep basins.

The accretionary prism (**Figures 1B,C**) is 20–30 km wide on average (Laurencin et al., 2019; Boucard et al., 2021), which is relatively narrow compared to its width in the south (~240 km,

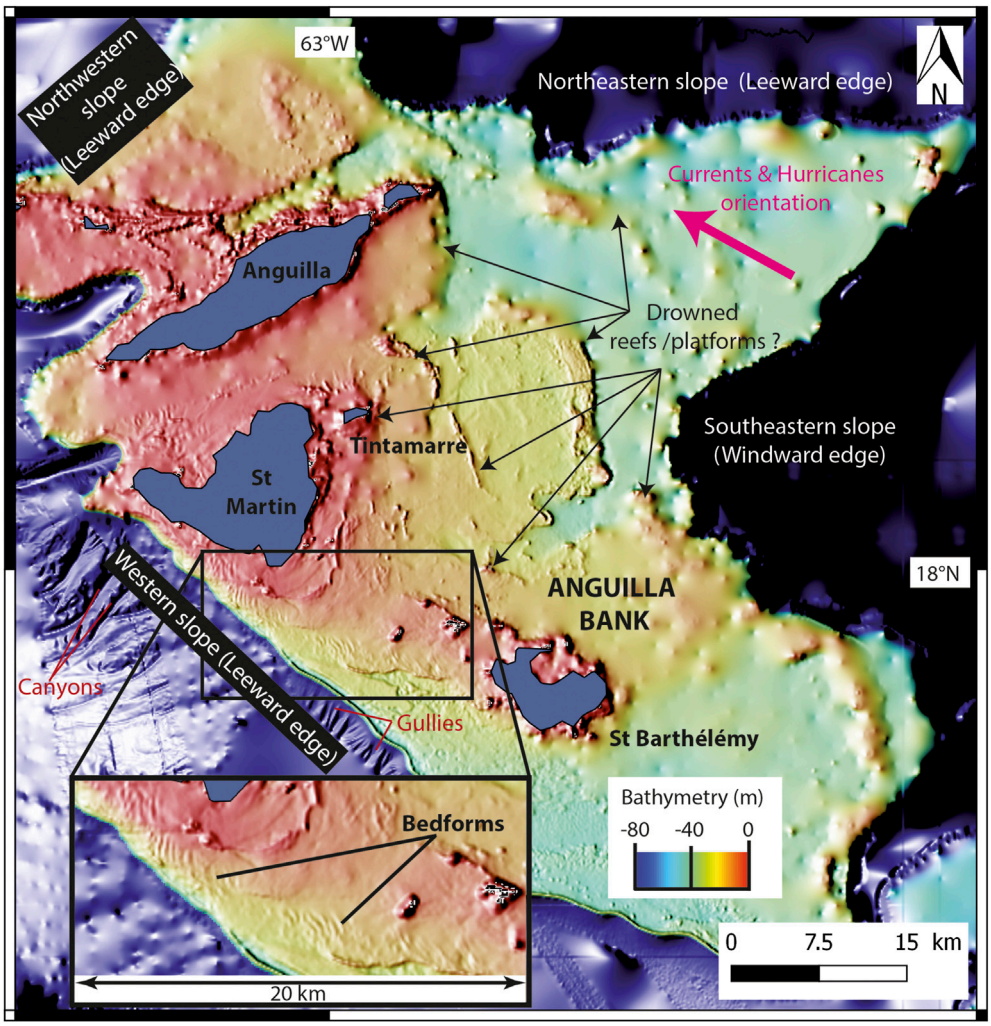

FIGURE 3 | Illustration of the Anguilla Bank with shallow-water bathymetry from the SHOM (2018). A sediment wave field on the shelf presents bedforms with an orientation N-S south of St Martin Island and NW-SE towards the St Barthélémy Island.

Seibert et al., 2020). The fold and thrust structure of the prism draws N120°-trending bathymetric linear features with positive elevation, which are parallel to the deformation front (Laurencin et al., 2019; Boucard et al., 2021). Northwestward, the accretionary prism is well delimited by the Bunce Fault (Laurencin et al., 2019); southeastward, this fault ends (black dots, **Figure 1B**) in an anastomosing system (Laurencin et al., 2019). With an average depth of 7,000 km, the trench (**Figures 1B,C**) has a flat bottom and a "U-form" morphology in front of the Barbuda-Anguilla segment (Laurencin, 2017). The trench presents variations in its depth and in its form eastwards and northwards (Laurencin, 2017).

2.3 Sedimentation and Climate

Pelagic carbonates, shallow-water carbonates redeposited by density cascading or gravity currents, and volcaniclastic silts and clays (including ashfall from the now inactive arc) represent the main sources of the deep-water sedimentation in the Lesser Antilles (Reid et al., 1996). Eolian dust from Africa represents another minor source (Reid et al., 1996). Distant sediment supply from the Orinoco delta is trapped by the accretionary prism and the ridges (Tiburón and Barracuda) and then confined in the trench (Deville et al., 2015). In the NLAS, sediment accumulation rates are relatively constant between glacial and interglacial periods, but vary significantly between the forearc and the arc platform, from 1 to 3 cm/kyr and more than 9 cm/kyr, respectively (Reid et al., 1996).

The Lesser Antilles are located in the tropical climate zone. They are exposed to large storms and tropical hurricanes, mostly between June and November (Saunders et al., 2017). In the NLAS, the mean orientation of the hurricane's tracks is similar to the subsurface submarine currents (**Figure 3**) oriented ESE-WNW to SE-NW (Richardson, 2005). According to Malaizé et al. (2011), periods of severe drought and hurricanes have alternated with periods of more uniform climate over the last 3,700 years. These variations are likely linked to the migration of the Inter-Tropical

Convergence Zone (ITCZ) combined with changes in the trajectory of cyclones (Bertran et al., 2004).

3 DATA AND METHODS

3.1 Data

This study is based on the analysis of geophysical data (backscatter and bathymetry) acquired during the ANTITHESIS 1 and ANTITHESIS 3 cruises (Marcaillou and Klingelhoefer, 2013; Marcaillou and Klingelhoefer, 2016) and of geophysical data (backscatter, bathymetry, MCS profiles, and sub-bottom profiles) from the CASEIS cruise (Feuillet, 2016) (**Figure 2**).

Backscatter and bathymetry data include Reson 7,150 multibeam echo sounder (MBS; 12 or 24 kHz) and 7111 MBS (100 kHz) acquired on board the *R/V POURQUOI PAS?* These data were complemented with Kongsberg-EM122 multibeam sounder bathymetry and backscatter data from the *R/V L'ATALANTE*. The horizontal resolution is 0.5 × 0.5° for the 24 kHz echo sounder (corresponding to ~25 m at about 3,000 m water depth and ~44 m at about 5,000 m water depth) and 1 × 1° for the 12 kHz echo sounder (corresponding to ~50 m at about 3,000 m water depth and ~85 m at about 5,000 m water depth).

Backscatter mosaic and bathymetric grids were produced using the IFREMER CARAIBES, GLOBE, and SONARSCOPE software. The grid size of the backscatter mosaics is 50 m for the 24 kHz mode in the study area. Grid size of bathymetry is about 20 m for high-frequency/shallow-water data and 50–100 m for low-frequency/deep-sea data. The bathymetric data of the Anguilla Bank (**Figure 3**) were acquired during the HOMONIM project (SHOM, 2018).

Forty-two multichannel seismic reflection profiles (48-traces) were acquired at 10 knots speed using a solid streamer with a shot interval of 50 m. Two GI guns were used as sources and covered frequencies between 50 and 150 Hz. The uninterpreted versions of the seismic reflection profiles are available in the supplementary material (**Supplementary Figures S1, S2**). Sub-bottom profiles were acquired with a hull-mounted source of 1.8–5.1 kHz and were processed using the SUBOP software (IFREMER).

3.2 Methods

Backscatter data are fundamental in reconstructing the sedimentary sources and pathways (Counts et al., 2018) and are shown in **Figures 4A,B**. Due to the strong heterogeneity of reflectivity, backscatter data were separated into different backscatter echo-facies characterized by their reflectivity level. As a result, the seafloor backscatter map (**Figure 4A**) was divided into five main echo-facies: [a] very high heterogeneous reflective (red), [b] high heterogeneous reflective (orange), [c] middle heterogeneous reflective (yellow), [d] low heterogeneous reflective (blue), and [e] very low heterogeneous reflective (dark blue), (**Figure 4B**). Highly reflective zones (light tones in **Figure 4A**, yellow areas in **Figure 4B**) are generally interpreted as active sediment transfer areas (Counts et al., 2018) such as canyons, gullies, or valleys where deposits are coarser, or alternately the areas where the seafloor is rougher, such as along scarps (Iacono et al., 2008). Low reflective zones (dark tones in **Figure 4A**, purple in **Figure 4B**) are generally interpreted as morphologically smooth, less active sedimentation areas (Counts et al., 2018), or areas of fine-grained sediment accumulation (Iacono et al., 2008).

A morpho-bathymetric map (**Figure 5**) was made from the available data although some areas were incomplete due to the lack of survey coverage (e.g., the outer arc or the insular slope). Detailed descriptions and interpretations were made from this map, from enlargements and seismic profiles (**Figures 6–11**). These descriptions are supported by morphometric quantification computed using QGIS software: areas of carbonate platforms and basins, width and length of structures, and the water depth range of all the features (**Table 1**). On maps of each insular slope (**Figures 6**, **8**, **9**), three canyons are highlighted to present their diversity in terms of length, form, and thalweg depth.

Along with the seismic profiles (**Figures 2**, **7**), we identified two main seismic facies [α] a facies with few reflectors and with no structure within or below, that we interpreted as the acoustic basement, and [β] a facies with continuous and parallel reflectors corresponding to stratified sedimentary deposits (interpretations based on principles developed by Payton, 1977). The nature of the acoustic basement is mostly volcanic as it is characterized by 4.7–6 km/s P-wave velocities (Laurencin et al., 2018) compatible with those of an uppermost volcaniclastic layer (Christeson et al., 2008; Kopp et al., 2011) and retrieved inland (Bouysse et al., 1985). Within facies [β], seismic units separated by unconformities are identified. We labeled them U1 to U5 (**Figure 10**) and Ua to Ud (**Figure 7B**) in the Anguilla and St-Barthélemy valleys, respectively. We used distinctive nomenclature for the units in both valleys since no temporal constrains allow correlating the units across valleys. The seismic facies [β] seems to be similar to the U4 sedimentary unit of Boucard et al. (2021), who interpret this unit as fan-shaped deposits filling the basins and the valleys. In the seismic facies [β], reflectors are often crosscut and offset by numerous faults (**Figure 7B**).

4 RESULTS: PHYSIOGRAPHY AND MAIN MORPHOLOGIC FEATURES OF THE NORTHERN LESSER ANTILLES SEGMENT (NLAS)

The seafloor of the NLAS (**Figure 5**) presents five morpho-structural areas: 1) the outer arc (from 0 to 1,000 mbsl), 2) the steep insular slopes (from 200 mbsl to 5,000 mbsl), 3) the forearc basin (from 5,000 mbsl to 7,000 mbsl), 4) the accretionary prism (from 5,600 mbsl to 5,900 mbsl) and 5) the trench (~7,000 mbsl). We focus the description of the area from the outer arc to the forearc basin, where the sedimentary sources, the turbiditic systems, and the distal sinks appear.

4.1 The Outer Arc and Carbonate Platforms

The outer arc consists of wide, relatively flat carbonate platforms lying on the old inactive volcanic arc at water depths shallower than ~100 m (**Figure 5**). The Anguilla Bank is the largest

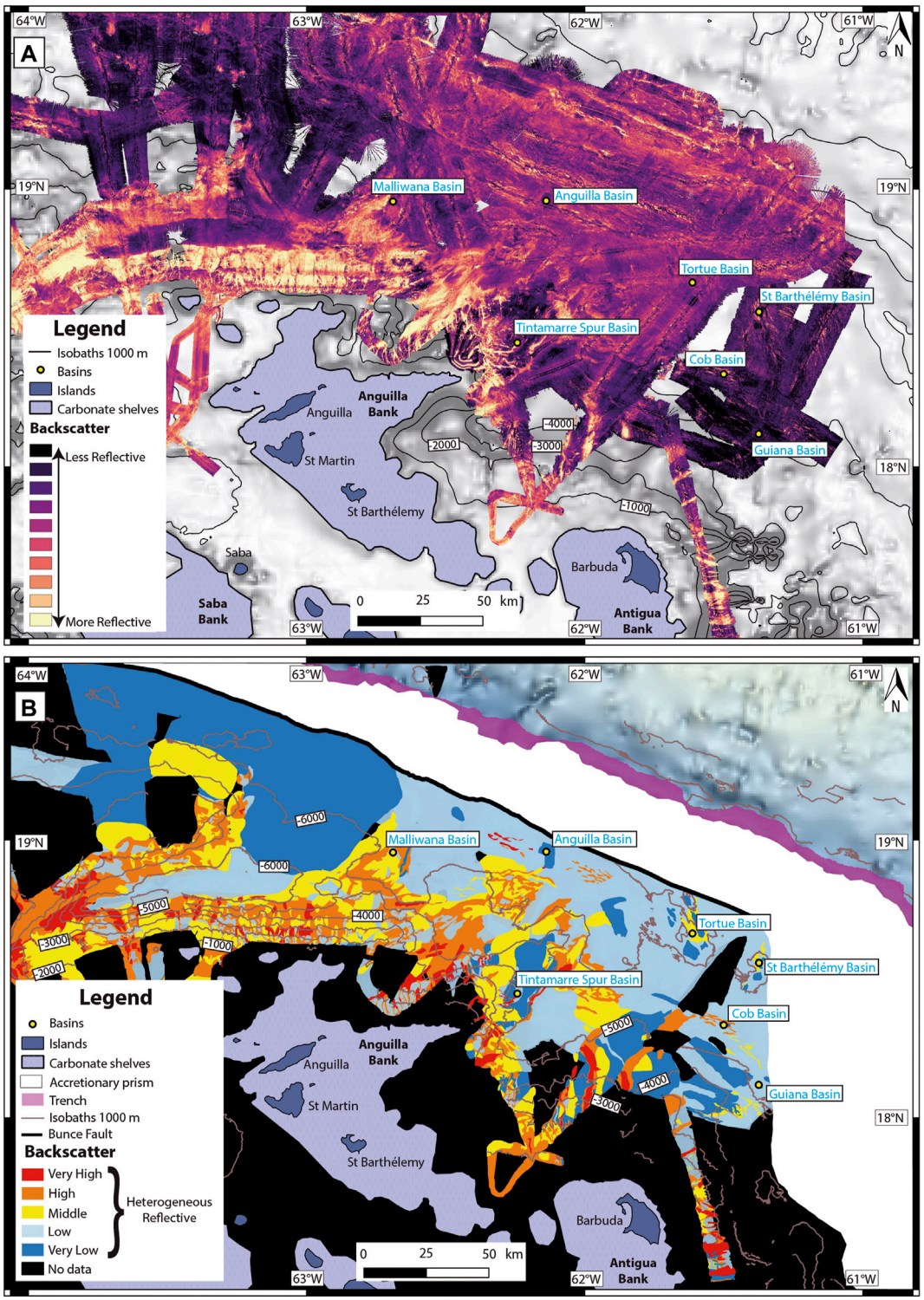

FIGURE 4 | Backscatter map: **(A)** Data (color scale plasma). **(B)** Interpretation. Five echo-facies: (a) Very High Heterogeneous Reflective (in red), (b) High Heterogeneous Reflective (in orange), (c) Middle Heterogeneous Reflective (in yellow), (d) Low Heterogeneous Reflective (in blue), (e) Very Low Heterogeneous Reflective (in dark blue). Please note that generally, highly reflective echo-facies (a,b) are present especially in the canyon floor and areas cut by gullies, the medium reflective facies highlight some valleys, and less reflective facies (d,e) are present in spurs and deep basins.

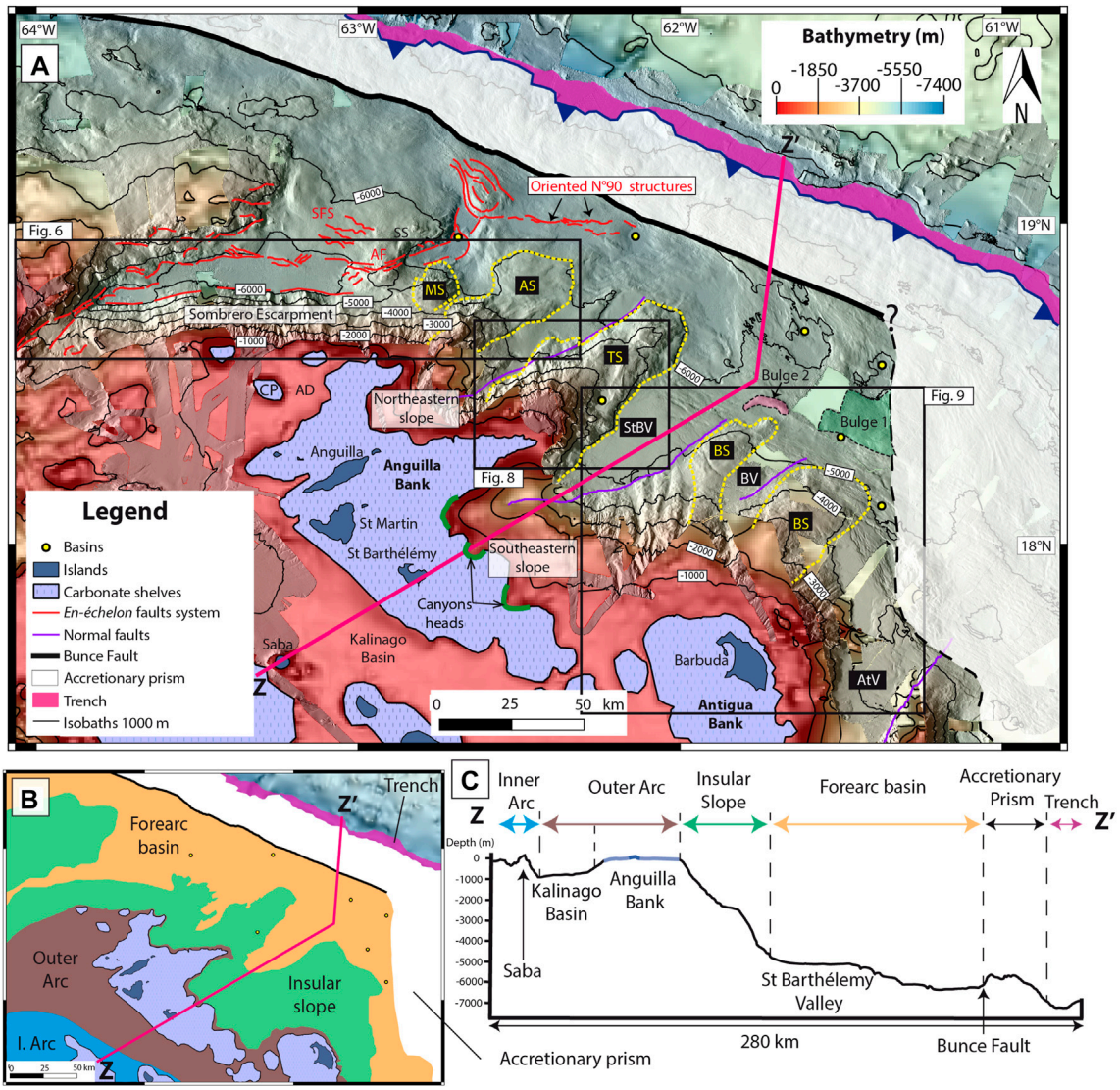

FIGURE 5 | (A) Morpho-bathymetric map of the NLAS. The cross-section AB is represented in pink in the main map and in the reduced map, it refers to **Figure 5B**). Red faults demarcate the Anegada Passage Eastern Segment, yellow dots indicate four main spurs. AB: Anguilla Basin, AD: Anguilla Depression, AF: Anguilla Faults, AS: Anguilla Spur, AV: Antigua Valley, BS: Barbuda Spur, BV: Barbuda Valley, CP: Crocus Platform, MS: Malliwana Spur, SFS: Sombrero Faults System, SS: Sombrero Saddle, StBV: St Barthélémy Valley, TS: Tintamarre Spur. **(B)** Reduced map of the main domains. **(C)** ZZ′ cross-section. The colors of the main domains double arrows are the same as in the insert map in **Figure 5B**).

carbonate platform (area of about 4,660 km^2, **Table 1**). The data reveals that the carbonate platform is not protected by shelf-edge barriers along most of its rim. Indeed, bathymetric highs are only visible east of Saint-Barthélémy and scarcely visible on the northeastern edge of the bank (**Figure 3**). However, the lack of multibeam coverage prevents precise mapping. Additionally, at ~40 mbsl, flat areas alternate with elongated highs rimmed at their seaward boundaries. We interpreted these successions of features as drowned platforms and reefs, as attested by previous studies (Christman, 1953; Cornee et al., 2021). Smaller carbonate platforms (30–53 km^2, **Table 1**) are also located north of the Anguilla bank in a 200-to-700-m-deep depression (Anguilla Depression, **Figure 5**; **Table 1**): Crocus (**Figure 5**; **Table 1**), Malliwana and Sombrero platforms (**Figure 6**; **Table 1**).

On the southern edge of the Anguilla Bank, south of Saint-Martin, ~2 m-high, ~400 m-long bedforms lie on the seafloor, trending N/S to NNW/SSE. The bedforms are observable to the western shelf edge and seem to be connected to NE-SW canyons incising the western slope of the Anguilla Bank. Given their shape and orientation perpendicular to the direction of the main submarine current (Richardson, 2005) (**Figure 3**), we interpreted these features as submarine dunes caused by the main currents (see Gonzalez and Eberli, 1997). The second-largest carbonate platform (area of about 3,800 km^2, **Table 1**)

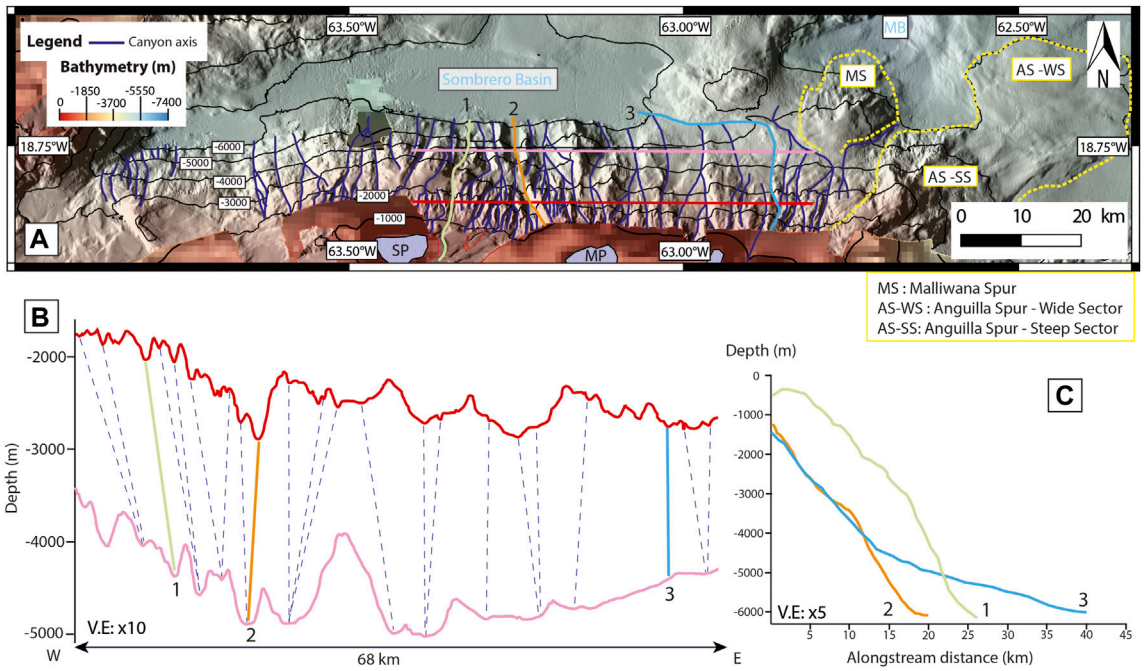

FIGURE 6 | (A) Enlargement of the Sombrero Escarpment. MB: Malliwana Basin, MP: Malliwana Platform, SP: Sombrero Platform. **(B)** W-E cross-section of the Sombrero Escarpment. The red cross-section is between 1,700 and 2,900 m and the light pink cross-section is between 3,500 and 5,100 m. Blue dots follow canyons axis between the two cross-sections. Three canyons axis (1, 2, and 3) are represented and referred to **Figure 6C**. **(C)** Bathymetric profiles of three canyons axis (1, 2, and 3).

is the Antigua Bank (**Figure 5**). However, we lack multibeam data to describe its detailed morphology.

4.2 The Insular Slopes

4.2.1 Sombrero Escarpment

The Sombrero Escarpment (**Figures 5A**, **6**) is oriented E-W with an average slope gradient of 14.7° and extends from 900 mbsl down to 6,000 mbsl. This escarpment is incised by numerous canyons (15–20 km long, up to 38 km for the longest, **Figure 6**), mostly linear and dipping northwards (**Figure 6A**) toward the Sombrero Basin. The shortest canyons present a 30 m-deep thalweg while the longest is up to 600 m-deep. For instance, canyons 1, 2, and 3 are representative of the erosional patterns on the Sombrero escarpment: Canyon 1 is a single and sinuous canyon presenting a continuous slope angle (~14,7°, **Figure 6C**). Canyon 2 is linear and merges with two northward-oriented tributary canyons between 2000 mbsl and 4,100 mbsl (**Figure 6C**). Canyon 3 is more sinuous and the longest, (38 km), merging with three S-N linear canyons between 5,000 mbsl and 6,000 mbsl. In their upper part, most canyons are slope-confined and show no connection with feeding channels from the Anguilla Depression (**Figure 5**). The canyons are highlighted by an alternation of highly reflective echo-facies [a] and [b], contrasting with less reflective facies [c] and [d] (**Figure 4B**, **Table 1**) in between. Given the high seafloor reflectivity within the canyons, we interpreted them as major sediment transfer paths as observed in similar contexts (Counts et al., 2018). The amount of sediment transfer is however probably limited given the disconnection with the upper slope.

4.2.2 Northeastern Slope of the Anguilla Bank

The northeastern slope of the Anguilla Bank, which extends from 100 mbsl down to 5,000 mbsl, is oriented NE-SW and shows a mean gradient value of 7.7° (**Figure 5**, **Table 1**). As observed along the Sombrero Escarpment, the northeastern slope of the Anguilla bank is incised by several canyons highlighted by reflective echo-facies [a] and [b] (**Figure 4B**, **Table 1**). Its northern tip, the Anguilla Spur (**Figures 5A**, **6A**), includes two sectors: a steep one (11.8°) from 2000 mbsl down to 5,000 mbsl, and an extended, wide sector (~550 km^2, 2.3°) from 5,000 mbsl to 6,000 mbsl.

In the Anguilla spur, seismic profiles reveal almost directly in the subsurface the acoustic basement (facies [α] in **Figure 7A**), with a limited number of discontinuous reflectors near the surface. Locally, a chaotic unit lies on top (enlargement in **Figure 7A**). We interpreted it as Mass Transport Deposit (MTD) (Weimer and Shipp, 2004), which attests to the occurrence of local destabilizations within the spur.

4.2.3 Tintamarre Spur

The Tintamarre Spur (**Figures 5A**, **8**) is a SW-NE trending structure located along with the eastward extension of the Anguilla Bank. The spur is slightly asymmetric, revealing a steeper mean gradient on its northwestern flank (12°) compared to the southeastern one (9.7°), most likely related to

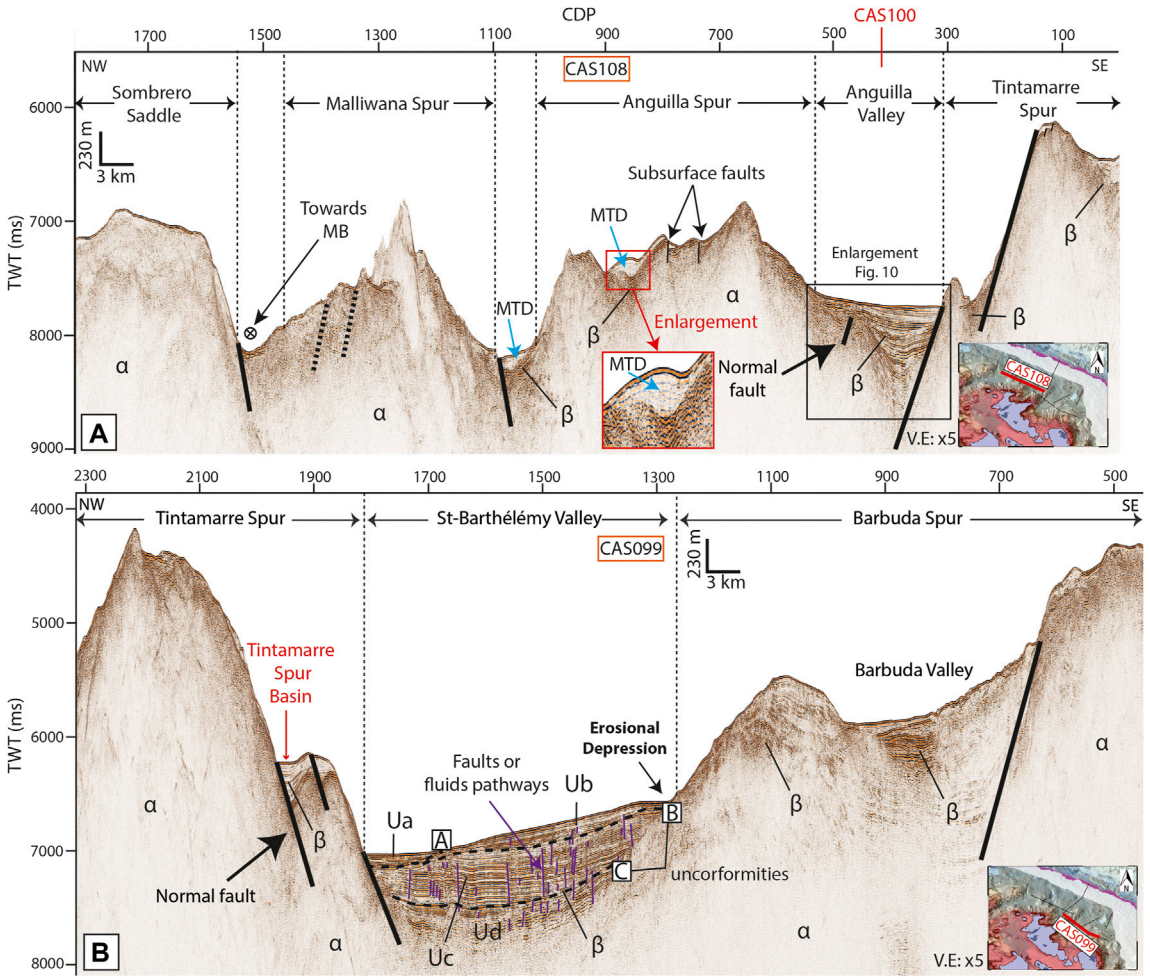

FIGURE 7 | Seismic profiles: **(A)** CAS108, uncertain faults are in dashed black. A, B, and C are unconformities, Ua to Ud are different seismic units. The black box locates an enlargement reporting to **Figure 10**; **(B)** CAS099. Acoustic facies in the seismic profiles [α] chaotic unit (acoustic basement) and [β] unit with evidence of numerous and stratified reflectors (basins, valleys). Red lines in the insert maps indicate the position of the seismic profiles. The vertical exaggeration (V.E) is x5 for the two seismic profiles.

the presence of normal faults on the western flank (Feuillet et al., 2002; and **Figure 7A**). The top of the spur reveals remarkable morphologies: two particularly planar and gently dipping surfaces (respectively ~2° and 4.5°) (**Figure 8**, **Table 1**), with an area of 37 and ~85 km^2, occur at ~700 mbsl and at ~1,600 mbsl. These features stand out from all other morphologies visible on the insular slopes, and we interpreted them as tilted strata. Given their location on the upper slope, at the edge of Anguilla Bank, these could be interpreted as subsided platforms (such structures have already been identified close to carbonate banks, Eberli and Ginsburg, 1987); we have named them paleo-platform PP1 and paleo-platform PP2 (**Figure 8A**).

On the northern part of the Tintamarre Spur, from 1,000 mbsl to 4,000 mbsl, numerous 10 to 18 km-long, northward-oriented canyons and/or gullies pour out into the Anguilla Valley (**Figure 8A**). These canyons/gullies are highlighted by the reflective echo-facies [a] and [b] while the rest of the spur is less reflective (echo-facies [c] to [e], **Figure 4B**, **Table 1**). Most canyons are slope-confined, with a spoon-shaped canyon head located at the edge of paleo-platform PP2 (**Figure 8A**). Similar headscarps also incise the edge of the upper paleo-platform PP1, with some gullies at its foot, streaming down to PP2. For instance, Canyons 4 and 5 incise both paleoplatforms *via* gullies in-between, while Canyon 6 is limited to PP2 (**Figure 8B**).

In the northeastern part of the Tintamarre Spur, from 4,000 to 6,000 mbsl, no canyon is identified. On the southeastern flank of the spur, only a few gullies and sinuous canyons occur (for instance Canyon 6 (Line 6, **Figure 8B**). Its slope gradient is locally steep between 1700 and 3,800 mbsl (14.5°), and decreases from 4,100 mbsl to 4,600 mbsl (11.9°). The canyon pours out in a relatively small slope basin located at 4,680 mbsl, (15 km^2, **Table 1**) called Tintamarre Spur Basin (**Figures 7B**, **8**). Its reflectivity is very low (echo-facies [e], **Figure 4B**, **Table 1**). It is highlighted by the seismic facies [β] on seismic profiles (**Figure 7B**). This basin is confined by the height of its flanks.

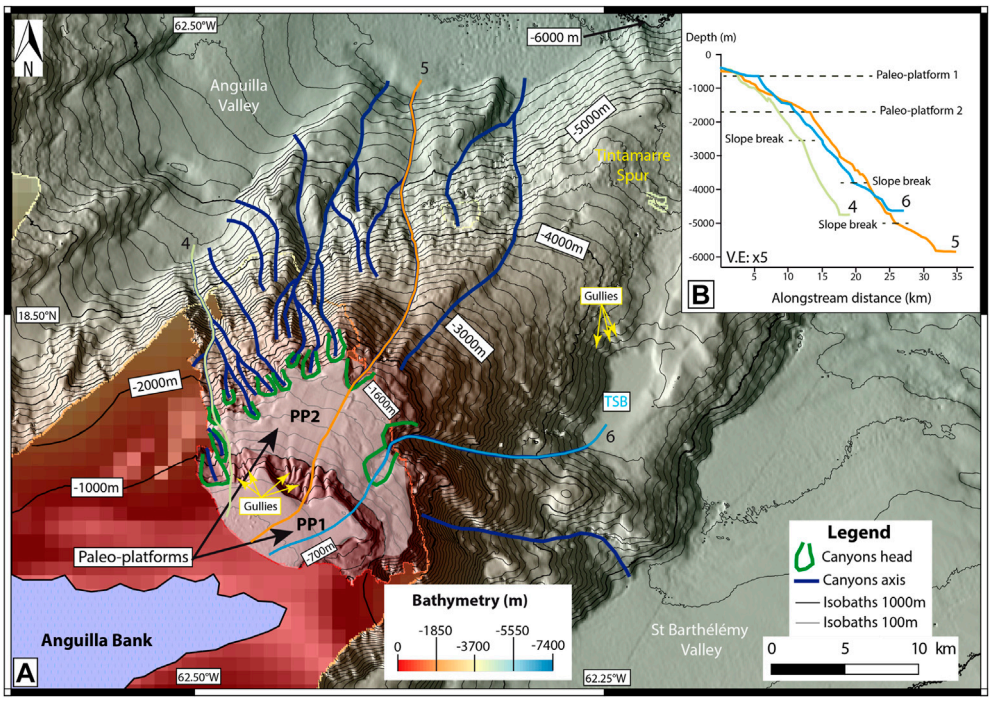

FIGURE 8 | (A) Enlargement of the Tintamarre Spur. PP1: Paleo-platform 1; PP2: Paleo-platform 2; TSB: Tintamarre Spur Basin. Three canyons axis (4, 5, and 6) are represented and referred to **Figure 8B**. Please note that canyons are more numerous in the northern part of the Tintamarre Spur than in the southern part. **(B)** Bathymetric profiles of three canyons axis (4, 5, and 6).

The southeastern slope of the Anguilla Bank (oriented NW-SE, **Figures 3**, **5**) is not imaged by multibeam data, but based on GEBCO Satellite bathymetry the shape of the 1000-m isobaths and some spoon-shaped (Canyons heads, **Figure 5A**) in the Anguilla Bank, which we interpreted as canyon heads, suggest the existence of SW-NE oriented canyons reaching the St-Barthélémy Valley.

4.2.4 Barbuda Spur and Valley

The northern slope of the Antigua Bank is composed of a major SW- NE trending spur called Barbuda Spur, cut by the 1000 m-deep Barbuda Valley (**Figures 5A**, **9**). The Barbuda Spur shows generally a low to very low reflective seafloor (echo-facies [d] and [e], **Figure 4B**, **Table 1**). With an average slope gradient of 5.7° from 120 mbsl to 5,000 mbsl, the SW-NE northern slope of Antigua Bank is also incised by northward oriented canyons, over 30 km long, 3 km wide, and ~500 m deep. The canyons, highlighted by echo-facies [a] and [b] (**Figure 4B**, **Table 1**), seem either slope-confined or connected at their head by gullies themselves connected upwards to the Antigua Bank (**Figure 9A**). These gullies are located downstream from passes across the reefs of Barbuda (yellow dashed arrows, towards gullies, **Figure 9E**). Four main canyons are visible between 4,000 mbsl and 5,000 mbsl (light pink cross-section, **Figures 9A,B**) and present a "U-shape". They result from the merger of other canyons between 1,500 mbsl and 3,500 mbsl. The 50-km-long canyon shown in line 7 (yellow line, **Figures 9B,D**) presents 400-m-high walls while the three other canyons have smaller walls, between 50 and 300 m (**Figure 9B**).

The Barbuda Valley has a depth of about 4,600 mbsl and is connected to the Antigua Bank through the main canyon (Canyon 8, **Figure 9A**) collecting sediment from several secondary canyons (**Figure 9D**). Between 2000 mbsl and 4,000 mbsl, where the secondary canyons spatially merge with the main one, the slope is steep (~7.4°) then flattens (~2.2°) below 4,000 mbsl (**Figure 9D**). The Barbuda Valley (**Figures 5A**, **9**) is highlighted by highly reflective echo-facies [a] and [b] (**Figure 4B**, **Table 1**) and is partially filled with stratified deposits illustrated by the seismic facies [β] on seismic profiles (**Figure 7B**). Additionally, the valley is bounded by a normal fault on its eastern flank (**Figure 7B**).

With an average slope gradient of 6.4°, the NNW-SSE oriented Antigua northeastern slope is incised by numerous and very reflective (echo-facies [a], **Figure 4B**, **Table 1**) SW-NE oriented linear canyons which are also linked to gullies at the top of the slope (**Figure 9**). With a length of at least 20 km, these narrow (<1 km width) canyons present 80-m-high walls between 2000 mbsl and 3,000 mbsl (orange cross-section, **Figure 9C**) and 10-to-100-m-high walls between 3,000 mbsl and 4,000 mbsl (brown cross-section, **Figure 9C**). They pour out onto a 4,000 mbsl deep terrace (**Figure 9**). Canyon 9 is linear and its thalweg presents an average slope of 10.1° between 1,000 mbsl and 4,000 mbsl.

To summarize, compared to the eastern flank, the north-western flank of the spur is dominated by a greater number of canyons, which moreover appear more incised and more reflective, probably supporting a more active sediment transfer as observed in other studies (Iacono et al., 2008; Counts et al.,

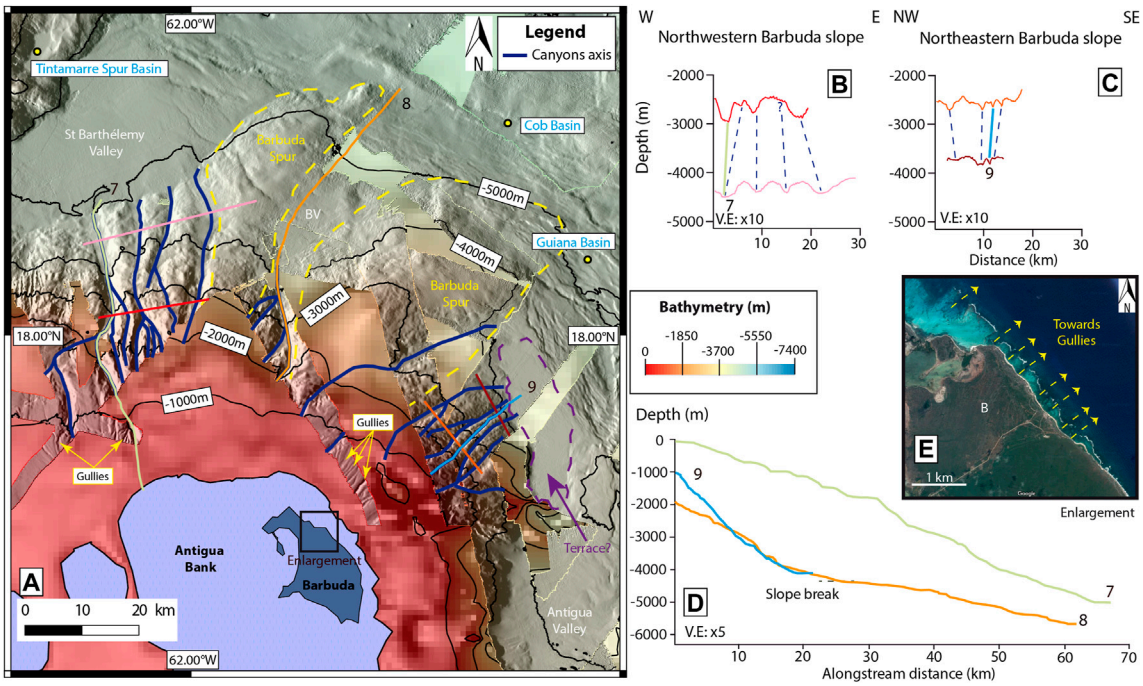

FIGURE 9 | (A) Enlargement of the northern slope of the Antigua Bank. BB: Barbuda Basin, BV: Barbuda Valley. Three canyons axis (7, 8, and 9) are represented and referred in **Figures 9B–D**. **(B)** W-E cross-sections of the northwestern slope of the Antigua Bank. The red cross-section is between 2,500 and 3,000 mbsl, the light pink cross-section is between 4,300 and 4,600 mbsl. **(C)** W-E cross-sections of the northeastern slope of the Antigua Bank. The orange cross-section is between 2,400 and 2,900 mbsl and the brown cross-section is between 3,700 and 3,900 mbsl. Blue dots follow canyons axis between the two cross-sections. **(D)** Bathymetric profiles of three canyons axis (7, 8, and 9). **(E)** Enlargement of Barbuda Island's passes. The Enlargement comes from Google Maps.

2018). The origins of these differences will be assessed in the discussion.

4.3 The Forearc

4.3.1 The Sombrero Basin

The Sombrero Basin, located at the toe of the Sombrero Escarpment, is 8 km wide and 86 km long, lying at ~6,200 mbsl (**Figure 6**; **Table 1**). This structure is bounded by transtensive faults (Laurencin et al., 2017). The seafloor is flat, and poorly reflective, highlighted by echo-facies [d] (**Figure 4B**). However, in front of the numerous canyons, the seafloor is slightly more reflective but still represented by the same echo-facies. We interpreted the infill as being either fine-grained (as observed by Iacono et al., 2008), and/or the sediment transfers being inactive, apart from in front of the canyons where accumulation is limited.

4.3.2 Deep Submarine Valleys

Two valleys are identified between the spurs: the Anguilla Valley (**Figures 5A**, **10**), delimited by the Tintamarre and Anguilla Spurs, and the St-Barthélémy Valley (**Figures 5A**, **10**), delimited to the SE by the Barbuda Spur. These two valleys, filled with stratified deposits illustrated by the seismic facies [β] (**Figures 7A,B**), are bounded by normal faults (Feuillet et al., 2002). Their seafloor however presents a contrasting backscatter signature (**Figure 10A**).

The Anguilla Valley, from 5,100 mbsl to 5,350 mbsl, (**Figures 5A**, **10**), is narrow (~10 km). In its distal part (**Figure 10B**), the seafloor is poorly reflective along the Tintamarre spur, while the axis of the valley and its distal vicinity is highly reflective (**Figure 10B**). This highly reflective seafloor correlates with truncated reflectors (**Figure 10C**). We interpreted these features as the presence of an active sediment transfer and erosional turbidity currents (active currents **Figure 10C**), as attested by the backscatter signature of turbidites in other studies (Iacono et al., 2008). Five units separated by four unconformities are visible in this valley (**Figures 10C,D**). U1 to U3 present continuous reflectors; U4 is more chaotic and onlaps in its southwestern part while U5 appears very chaotic, with few strong and parallel reflectors. U1 and U4 share a similarity: an erosive depression is visible in U1 at the foot of the slope, and a similar buried feature is identified in U4 (**Figure 10D**).

Conversely, the St-Barthélémy Valley (**Figures 5A**, **7–10**) is a broader submarine valley (~28 km wide, 4,900–5,200 mbsl) presenting a low reflective seafloor (**Figure 10A**, echo-facies [d], **Figure 4B**; **Table 1**) compared to the Antigua valley. At the foot of the southeastern slopes off the Anguilla Bank, the seafloor is locally more reflective (echo-facies [a] to [c], **Figure 4B**, **Table 1**) describing a lobate shape (Lobate Structures, **Figure 10**). The infill of the valley is well stratified and shows at least 4 units (Ua to Ud) separated by three unconformities (A to C in **Figure 7B**). The most recent infill shows well-stratified reflections (**Figure 7B**), lying unconformably on top of truncated reflectors. We interpreted the sediment transfer within the valley as being less active and/or comprising finer-grained deposits than within the Anguilla valley (as observed in other studies (Iacono et al., 2008; Counts et al., 2018).

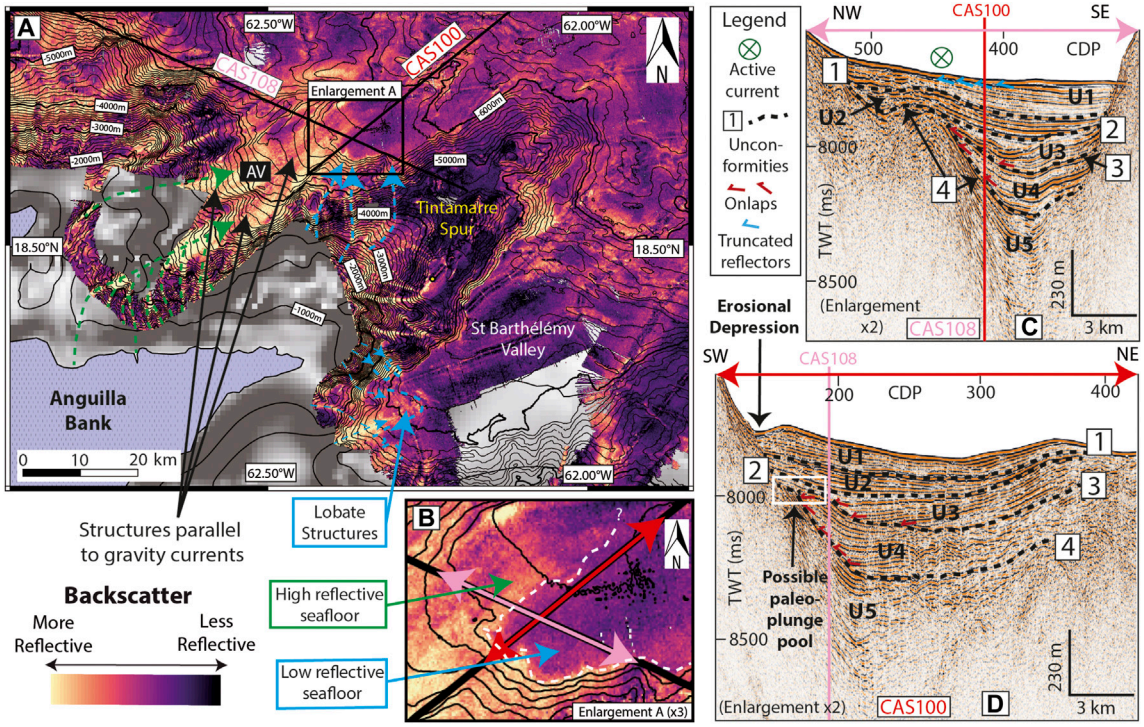

FIGURE 10 | Enlargement of the two main valleys. **(A)** Interpreted backscatter map. Blue dashed arrows represent sediment transfer from the northeastern Anguilla Bank. Blue dots delimit lobate structures in the St-Barthélémy Valley. Green dashed arrows represent sediment transfer from the paleo-platforms of the Tintamarre Spur. AV: Anguilla Valley. Please note that the backscatter pattern is totally different between the two valleys. **(B)** Enlargement of **Figure 10A**. The light pink double arrow locates the enlargement C coming from the seismic line CAS108 (**Figure 7A**). The red double arrow locates the enlargement D coming from the seismic line CAS100. The white dots separate the active transfer area (indicated by a green arrow) and the transfer and deposition area (indicated by a blue arrow). **(C)** Enlargement of the seismic line CAS108 (**Figure 7A**). The red line indicates where the seismic line CAS100 cut the seismic line CAS108. The vertical exaggeration is x5 for the seismic profile. **(D)** Enlargement of the seismic line CAS100. U1 to U5 refers to the number of units. The light pink line indicates where the seismic line CAS108 cut the seismic line CAS100. The vertical exaggeration is x5 for the seismic profile.

The presence of unconformities in both valleys suggests successive periods of sediment transfer (as attested by other studies, e.g. Laban et al., 1984) but also at least one subsidence phase, attested by the divergent geometry of the reflectors of U3, U4, and U5 in the Anguilla Valley. Drastic subsidence in the area has already been identified on MCS profiles (Boucard et al., 2021), suggesting the importance of tectonics in the Northern Lesser Antilles Segment.

4.3.3 Plunge Pools

In the St-Barthélémy Valley, erosional depressions (**Figures 7B**, **11**) occur along the 5,000 m isobaths and are located at the foot of the northern slope of the Antigua Bank (**Figure 11A**). They are 540–1,200 m long and 16–20 m deep, where the slope break ranges from 4° to 7° (**Figures 11B–E**). In detail, sub-bottom profiles reveal a small, highly reflective depression located at the foot of the slope, with a mounded shape located immediately basinward from the depression (**Figure 11B**). The mound shows stratified acoustic facies with low amplitude continuous reflectors. A similar structure, visible in the Anguilla Valley (**Figure 10**), is 1,450 m long and 22 m deep, at a break in slope of ~7°and corresponds to the erosive depression associated with U1 (**Figure 10D**). Due to their stratified composition with low amplitude continuous reflectors, corresponding to alternating fine- and coarse-grained material (e.g., Hassoun et al., 2009), we inferred that these features have a sedimentary origin. We interpreted these features as plunge pools, characterized by an erosional scour at the foot of a steep slope, and a depositional slope-break deposit downstream (Komar, 1971; Mulder and Alexander, 2001; Lee et al., 2002; Bourget et al., 2011; Migeon et al., 2012). Given their similarities, we interpreted the erosional and depositional features described at the slope break in Units U1 and U4 (**Figure 10D**) as active and buried plunge pools, respectively.

4.4 Deep Basins and Seismic Stratigraphy of Basin Fill

The study of deep sub-basins helps to determine the occurrence–or not–of sediment transfer and deposition in the area. Several forearc sub-basins have been identified, from 5,000 mbsl to 7,000 mbsl (**Figure 5**). They are dominated by low reflective seafloor or echo-facies [d] to [e] (**Figure 4B**, **Table 1**), implying mostly fine-grained sediment accumulation (Counts et al., 2018). Seven basins or sinks of varying geological contexts in this area are illustrated by sub-bottom profiles and are in different geological contexts. Groups of black reflectors alternating with transparent and thick units are visible on the sub-bottom profiles (**Figure 12**). The proximal sub-

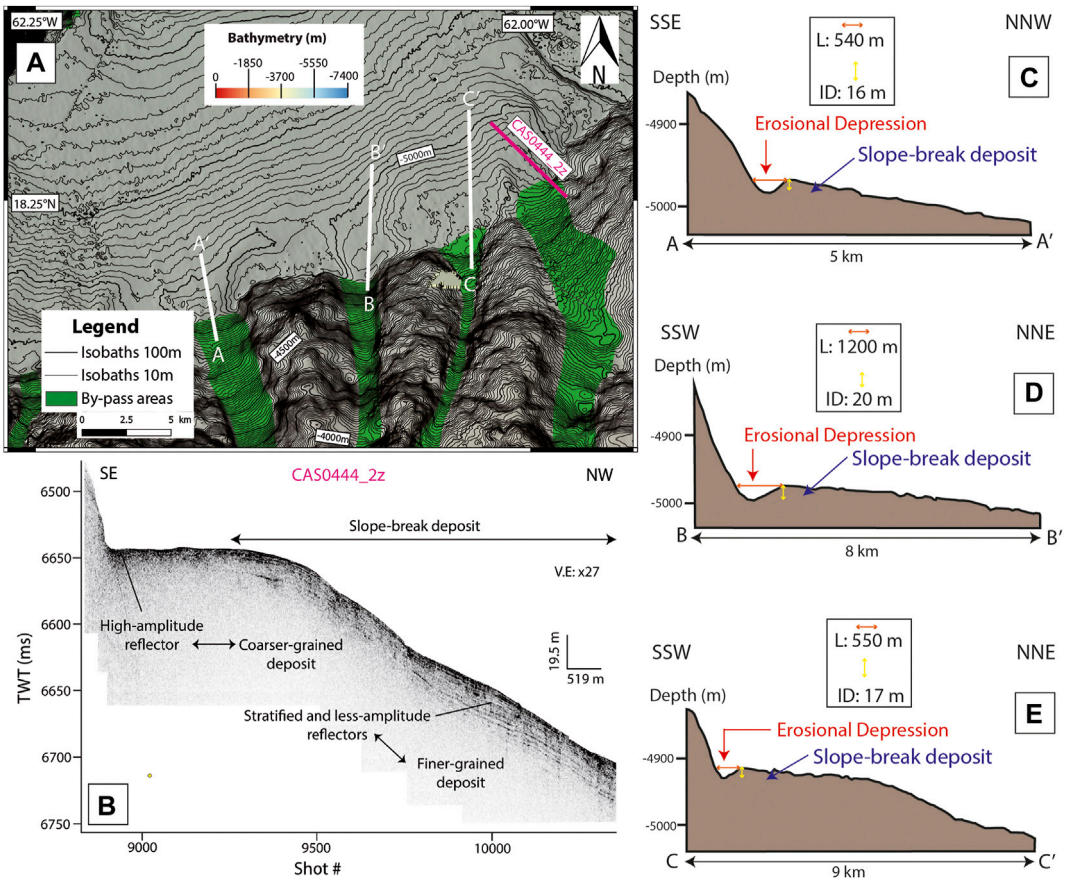

FIGURE 11 | (A) Identification of unusual sediment structures in the St-Barthélémy Valley. These structures are illustrated in a sub-bottom profile and in three cross-sections. **(B)** Enlargements on sub-bottom profile CAS0444_2z. The enlargement was realized using QC SBP5.0_64bits (Ifremer, Brest). **(C)** Cross-section AA′ **(D)** Cross-section BB′ **(E)** Cross-section CC′. L = Length, ID = Incision Depth for the Erosional Depression.

basins (Guiana Basin, Cob Basin, and Tintamarre Spur Basin) contain at least one thick transparent unit, while the distal sub-basins contain at least two thick transparent units (**Figure 12**):

- the Guiana Basin (**Figures 4**, **9**, **12A**, **13**) and the Cob Basin (**Figures 4**, **9**, **12B**, **13**) are small sinks (~3 km^2, **Table 1**) located close to the insular slope at 5,150 and 5,800 mbsl, respectively (**Table 1**).
- the St-Barthélémy Basin (~10 km^2, **Table 1**) and the Tortue Basin (~17 km^2, **Table 1**) are basins at great depth (~6,100 mbsl, **Table 1**), located close to the accretionary prism and far from the slopes of the Antigua Bank (**Figures 4**, **12C**,D, **13**).
- the Tintamarre Spur Basin (**Figure 12E**) is a small slope-confined basin (~15 km^2, **Table 1**) located on the Tintamarre Spur (**Figures 4**, **7B**, **8**, **13**) at 4,600 mbsl (**Table 1**).
- the Anguilla Basin (**Figure 12F**) is larger (~45 km^2, **Table 1**) and deeper (~6,700 mbsl, **Table 1**) than the previous basins and is located close to the accretionary prism and far from the slopes of the Anguilla Bank (**Figures 4**, **13**).
- the Malliwana Basin (**Figures 12G,H**) is a wide (~155 km^2, **Table 1**) and deep (~6,900 mbsl, **Table 1**) pull-apart basin located close to the northeastern slope of the Anguilla Bank (**Figures 4**, **6**, **13**) in an *en-échelon* fault system (Laurencin et al., 2018). In this basin, another acoustic transparent unit is visible in the subsurface of the basin but does not fill the entire basin (**Figure 12H**). This unit seems to be correlated with a spoon-shaped structure visible on the backscatter (**Figure 12G**). Thus, at around 5,000 mbsl, in the Malliwana Spur, some semi-circular structures are observable (**Figure 12G**). We interpreted these structures as evacuation areas (see Moscardelli and Wood, 2016) while the spoon-shaped structure could be interpreted as an MTD, suggesting local destabilizations on the Malliwana Spur. It also implies different triggering mechanisms for the MTD and the others megabeds filling the entire surface of the basin.

Acoustically transparent and thick units identified in sub-bottom profiles are similar to units identified elsewhere and called the term "unifite" (Stanley, 1981), then megaturbidites (San Pedro et al., 2017), or homogenites (Kastens and Cita, 1981; Beck, 2009; Beck,

TABLE 1 | Main characteristics of the structures of the Norther Lesser Antilles Segment.

Physiographic domain	Detail zone	Structures	Ab.	Water depth range (m)	~Area (km^2)	Length (km)	Width (km)	Backscatter echo-facies	Related figures
Outer Arc		Kalinago Basin	KB	200–800	—	200	20	d	1b, 5, 13
		Anguilla Bank	AngB	0–100	4,660	110	40	ND	1b, 2, 3, 5, 8, 13
		Antigua Bank	AntB	0–200	3,800	90	45	ND	1b, 2, 5a, 9, 13
		Crocus Platform	CP	35–180	53	11	7	ND	5a, 13
		Malliwana Platform	MP	35–150	30	8.5	5.2	ND	6, 13
		Sombrero Platform	SP	2–20	33	9	5.3	ND	6, 13
Insular Slope	Northern slope	Sombrero Escarpment	—	200–6,000	—	90	—	a to b (canyons) c to d (interfluves)	5a, 6
		Malliwana Spur	MS	4,000–6,000	150	~15	10 to 15	b to d	6, 7a, 13
	Anguilla Bank slopes	Northeastern slope	—	100–5,000	—	~50	—	a to b	3, 5a
		Anguilla Spur	AS	2000–6,000	900	~40	15 to 26	b to d	6, 7a, 13
		Tintamarre Spur	TS	1,000–6,000	2000	~60	35–22	a to c (upper spur) c to e (lower spur)	1b, 7a, 7b, 8, 10, 13
		Tintamarre Spur Basin	TSB	4,600	15	7	2.5	d	7b, 8, 9, 12, 13
		Southeastern slope	—	100 to 5,000	—	~70	—	ND	3, 5a, 5b
	Antigua Bank slopes	Barbuda Spur (NW)	BS	120 to 5,000	670	37	10 to 16	d to e	1b, 7b, 9, 13
		Barbuda Spur (SE)		120 to 5,000	1,070	40	28		7b, 9, 13
		Barbuda Valley	BV	4,600	—	~30	5	a to c	7b, 9, 13
		Northwestern slope	—	120 to 5,000	—	36	—	a to b (canyons)	9
		Northeastern slope	—	120 to 5,000	—	21	—	c to d (interfluves	9
Forearc	Northwestern forearc	Anguilla Valley	AngV	2000 to 6,000	—	~50	10	a to c (shallower valley) c to e (deeper valley)	1b, 7a, 8, 10, 13
		Sombrero Basin	SB	6,000 to 6,400	905	86	8	d	6, 13
		Malliwana Basin	MB	6,800 to 7,000	145	18.5	8.5	c to d	6, 12, 13
		Anguilla Basin	AB	6,700	45	10	8.5	d	5a, 12, 13
	Southeastern forearc	StBarthélémy Valley	StBV	4,900 to 5,200	—	~65	28	c to d	1b, 5b, 7b, 8, 9, 10, 11, 13
		Guiana Basin	GB	5,150	3	3.5	1	d	4, 9, 12, 13
		Cob Basin	CB	5,800	3	2.5	1	d	4, 9, 12, 13
		St Barthélémy Basin	StB	6,100	10	4	2	d	4, 12, 13
		Tortue Basin	TB	6,110	17	7	2	c	4, 12, 13
		Antigua Valley	AntV	4,000	—	~85	17	ND	9

The two values of width of the spurs correspond respectively to the width of the upper spur and the width of the lower spur, and backscatter echo-facies refers to ***Figure 4****.*

2012; Polonia et al., 2017; San Pedro et al., 2017; McHugh et al., 2020). Without sedimentological analysis to decipher their nature, we called these units "megabeds" (**Figure 12**).

5 DISCUSSION

The study area presents evidence of sediment transfer, identifiable despite the absence of deep-sea channels in the forearc basin thanks to highly reflective seafloor in the Anguilla Valley (**Figure 10A**), reflective lobate patches in the St-Barthélémy Valley (**Figure 10A**), plunge pools (**Figures 7B**, **10D**, **11**), MTDs (**Figures 7A**, **12D,H**), and megabeds in the deep basins (**Figure 12**). This evidence implies the occurrence of gravity processes (slope failures, density currents, etc.). To infer controls on the sediment transfer and tentatively the nature of deposits, we discuss the present-day links between morphology and sediment transfer, deduce the nature of deposits and the type

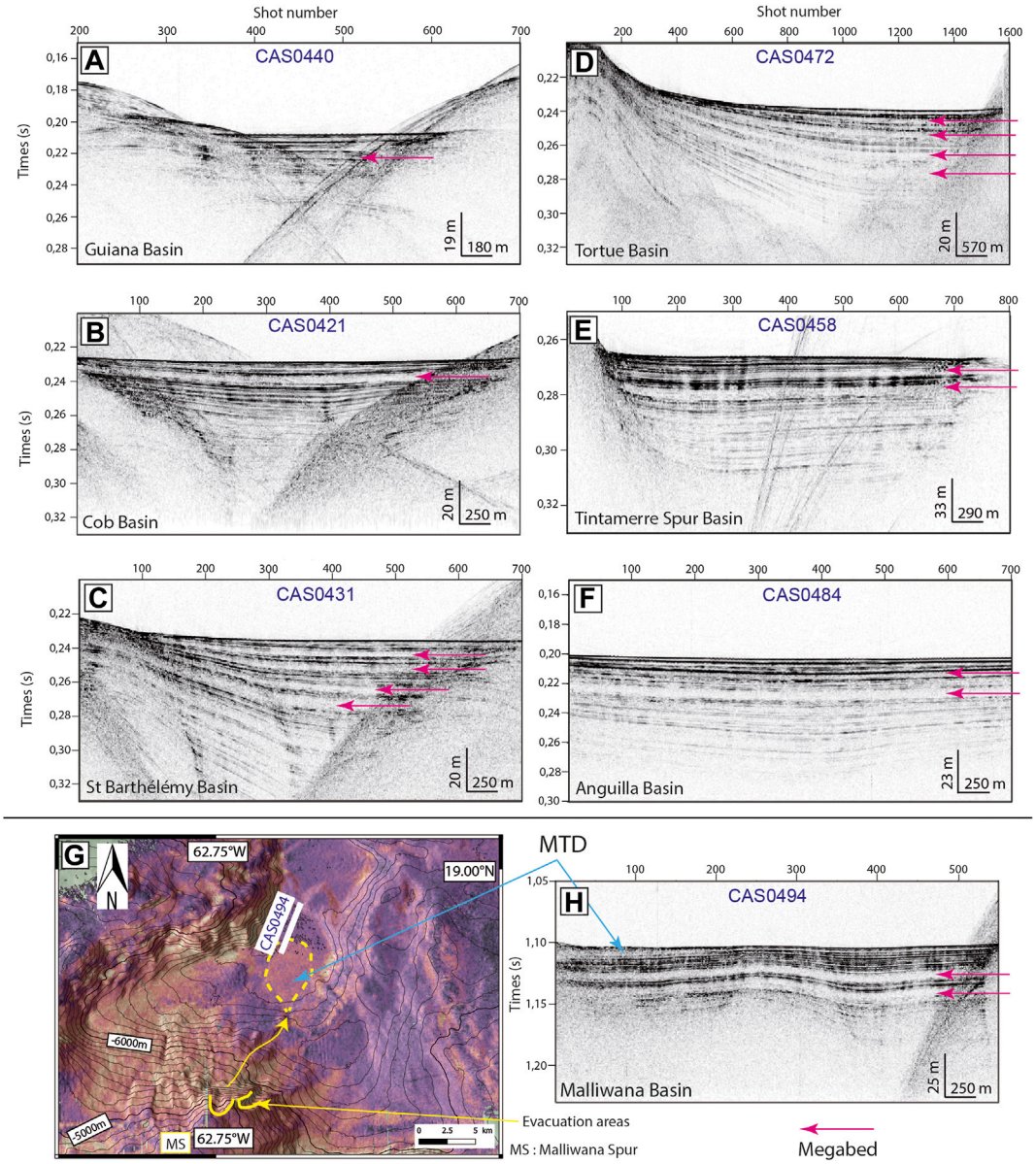

FIGURE 12 | Identification of thick acoustically transparent units in the sub-bottom profiles of the basins. Numerous thick "acoustic megabeds" can be identified but only the most visible are highlighted by the arrows. **(A)** Guiana Basin. **(B)** Cob Basin. **(C)** St Barthélémy Basin. **(D)** Backscatter map of the Malliwan Basin. Yellow dotted line highlights a MTD. **(E)** Tortue Basin. **(F)** Tintamarre Spur Basin. **(G)** Anguilla Basin. **(H)** Malliwana Basin. The basins are located in **Figures 4**,**13**. MTD: Mass-Transport Deposit.

of mixing, and discuss the longer-term (Kyr to Myr) external controls on these systems.

5.1 Morphological Factors Influencing the Sediment Transfer

5.1.1 Connection Between Canyons and Reef Passes

The northeastern slope of Antigua Bank (**Figure 9**) is the only area illustrating a direct spatial relation between reef passes, gullies, and canyons (Sedimentary system 1, **Figure 13A**, **Table 2**). The northeastern edge of Barbuda Island shows a narrow fringing reef disrupted by a series of passes visible in satellite photographs (**Figure 9E**). Relatively large gullies are identified on the upper slope in front of the passes (**Figure 9A**), likely acting as pathways for sediment flux. Such features are very similar to those observed off the Bahamas Banks (Mulder et al., 2017; Fauquembergue et al., 2018). They most likely result from sediment resuspension in the lagoon during cold fronts and hurricanes, leading to sediment export by density cascading and ebb currents (Wilson and Robert, 1995; Mulder

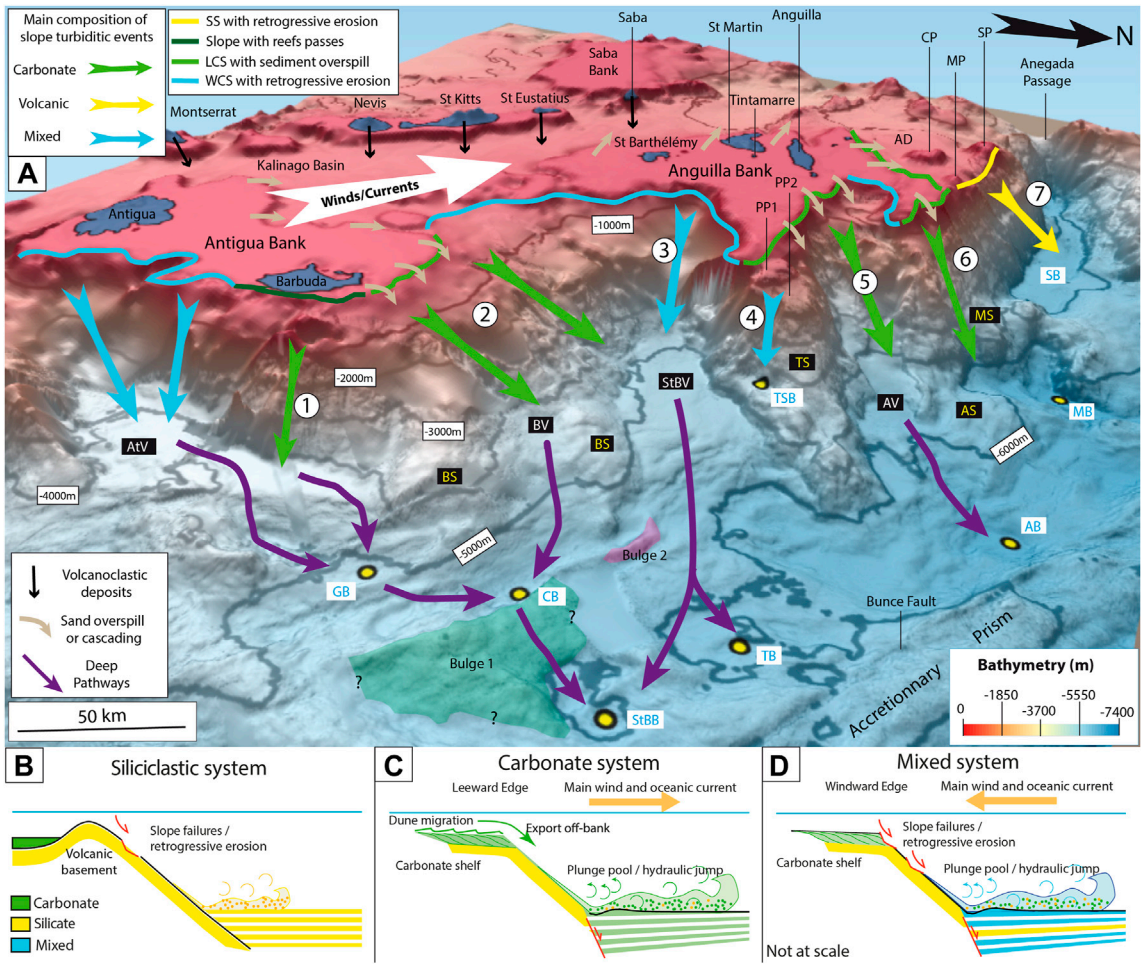

FIGURE 13 | (A) 3D block diagram identifying the nature of the sources of the turbidity currents and the associated mechanisms. Purple arrows correspond to the main deep pathways. The numbers (1–7) refer to the name of the sedimentary systems in Tab.2. Legend of the slopes: LCS: Leeward Carbonate Slope, SS: Siliciclastic Slope, WCS: Windward Carbonate Slope. AB: Anguilla Basin, AD: Anguilla Depression, AS: Anguilla Spur, AV: Antigua Valley, AV: Anguilla Valley, BB: Barbuda Basin, BS: Barbuda Spur, BV: Barbuda Valley, CP: Crocus Platform, MB: Malliwana Basin, MP: Malliwana Platform, MS: Malliwana Spur, PP1: Paleo-Platform 1, PP2: Paleo-Platform 2, StBV: St-Barthélémy Valley, SB: Sombrero Basin, SP: Sombrero Platform, TS: Tintamarre Spur. The Vertical Exaggeration is x5. **(B)** Scheme of a siliciclastic sedimentary system dominated by volcanic input. **(C)** Scheme of a sedimentary system dominated by carbonate input. **(D)** Scheme of a sedimentary system with mixed input.

et al., 2017). This direct connection between the Anguilla Bank and the slope implies a carbonate source due to the carbonated nature of the bank (Christman, 1953).

5.1.2 Orientation of Shelf Edges with Respect to Winds and Currents

The orientation of the carbonate platforms and shelf edges with respect to major winds and oceanic currents plays an important role in sediment transfer down to deep basins (Gonzalez and Eberli, 1997; Rankey et al., 2006; Counts et al., 2018). In the study area, the Anguilla Valley is located in the continuity of canyons incising the northeastern slope of the Anguilla Bank (**Figure 10**), which represents a leeward (i.e. downwind) edge of the bank (**Figure 3**). The Anguilla Valley seafloor is highly reflective (**Figure 10**), likely indicative of coarse sediment and/or efficient sediment transport. Upstream, numerous bedforms, that we interpreted as submarine dunes are detectable along the western part of the Anguilla Bank (**Figure 3**). They suggest a westward migration of carbonate sands, in accordance with the main direction of the Caribbean oceanic current and winds (Richardson, 2005). The shelf edge is favorably oriented for sediment overspill caused by dominant currents, and the bedforms seem to migrate off-platform (**Figure 3**). They thus most likely constitute a source of sediment supply as documented in other regions (Gonzalez and Eberli, 1997; Jorry et al., 2016; Counts et al., 2018). The presence of numerous canyons located directly at the shelf break supports this interpretation (**Figure 3**). We therefore infer, by analogy, that sediment overspill is a major process for sediment delivery on the east of the Anguilla Bank (beige arrows, **Figure 13A**). This implies the remobilization of carbonate sediment and its transport from the Anguilla Bank to the slope (**Figure 13A**).

TABLE 2 | Identification of sedimentary systems (or turbiditic systems) and their nature (siliciclastic/carbonate/mixed) based on morphological and reflectance evidences.

Name of the sedimentary system (nb)	Elements	From (mbsl) to (mbsl)	Total length (km)	Av. slope (°)	Comments/evidences	Interpretation
NE Antigua Bank (1)	Lagoon, passes, gullies canyons	100–5,000	95 (until CB)	6.4	The only continuous system reef to deep sea	Carbonate (mainly)
NW Antigua Bank (2)	Canyons	100–6,000	105 (until StBB and TB)	5.7	Plunge-pools in St Barthélémy Valley	Carbonate (mainly)
SE Anguilla Bank (3)	Rare canyons	100–6,000	140 (until TB)	—	—	Mixed
Tintamarre Spur (4)	Gullies	700–4,600	20 (until TSB)	—	Local system	Mixed
NE Anguilla Bank (5)	Canyons	100–7,000	110 (until AB)	7.7	Anguilla Valley	Carbonate (mainly)
N Anguilla Bank (6)	Canyons	100–7,000	100 (until MB)	—	—	Carbonate (mainly)
Sombrero Escarpment (7)	Canyons	900–6,000	20 (until SB)	14.7	—	Siliciclastic

*The number of each sedimentary system refers to **Figure 13**; AB, Anguilla Basin; CB, Cob Basin; MB, Malliwana Basin; SB, Sombrero Basin; StBB, St-Barthélémy Basin; TB, Tortue Basin; TSB, Tintamarre Spur Basin.*

A similar configuration, with a shelf edge favorably oriented for overspill and canyons located downslope, exists off the northwest Antigua Bank (Sedimentary system 2; **Figure 13A**, **Table 2**). However, the Barbuda and Saint-Barthélémy valleys located downwards present a less reflective seafloor, likely transferring less or finer-grained sediment (Counts et al., 2018) compared to the Anguilla Valley. This fining is probably due to the greater distance (~50 km, **Figure 9**) of the canyon heads from the shelf break, but also to the gentler slope gradient, which could favor deposition rather than transport.

The southeastern slope of the Anguilla Bank presents an opposite configuration, being located off a windward edge (i.e., facing the wind; **Figures 3**, **13A**). In this sediment system, canyon heads have been identified on the platform edge (**Figure 5A**) and numerous highly reflective lobate patches are found in the downstream reaches of the St-Barthélémy Valley (**Figure 10**). Due to their high to medium reflectivity (**Figure 10A**), these features are interpreted as coarse-grained deposits, located close to the slope break. Given their lobate structure and based on other case studies, they could be interpreted as MTDs (Moscardelli and Wood, 2016) or submarine fans (Shanmugam, 2016).

5.1.3 Retrogressive Erosion on the Slopes

Retrogressive erosion is a common process on submarine slopes in siliciclastic (Pratson et al., 1994; Pratson and Coakley, 1996), carbonate (Tournadour et al., 2017), or mixed sedimentary systems (Puga-Bernabéu et al., 2011). This process mainly affects the slopes disconnected from any input from the carbonate banks, for example on the Sombrero Escarpment or the Tintamarre Spur (**Figures 6**, **8**).

The Sombrero Escarpment (**Figure 6**) is incised by numerous submarine canyons that are not directly connected to the Anguilla Bank. It is separated from the Anguilla Bank by the ~60-km-wide Anguilla Depression located below the storm-wave base (300 mbsl), where waves generate no water motion (Peters and Loss, 2012 and references therein), preventing the entrainment of sediment particles down the canyons of the Sombrero Escarpment. The Sombrero Escarpment canyons are mostly slope-confined and disconnected from any feeding channel. Additionally, a ~100 m-high bathymetric elevation at the edge of the Anguilla Depression (**Figure 5C**) most likely acts as a dam, preventing sediment overspill onto the slope. The canyons incise the seafloor composed of volcanic basement or mostly volcaniclastic deposits as attested by dredged rocks collected along the escarpment (Bouysse et al., 1985) supporting that the deposits transferred within this siliciclastic system derived from volcanic sources. The low reflectivity downstream of the canyons (**Figure 4**) suggests that the deposits are probably fine-grained, but also that the sediment transfer is limited.

On the Tintamarre Spur (Sedimentary system 4, **Figure 13A**, **Table 2**), two paleo-platforms are situated at 700 mbsl and 1,600 mbsl (**Figure 8**). Between the shallowest paleo-platform and the shelf edge, no gullies, no bedforms, and no areas of high reflectivity are identified, suggesting that there is no sediment transfer from the Anguilla Bank at the moment. Both paleo-platforms show a gently dipping surface (2.4–6.6°), with a sharp slope break (16.6–18.6°) affected by spoon-shaped head scarps with gullies and canyons downwards. Due to the absence of connection with the Anguilla Bank, these canyons were probably formed by retrogressive erosion.

5.1.4 Role of Slope Gradient on the Distribution of Canyons and Plunge Pools

Many canyons (and gullies) are clearly identified on the steep insular slopes of the NLAA (**Figures 6**, **8–11**), but they are generally scarcely incised and slope-confined. This diffuse distribution leads to the presence of multiple but relatively small point sources along the insular slopes. The canyons feed the foot of the slope, resulting in a scattering of sediment fluxes, which, combined with the very low accumulation rates (from 1 to 3 cm/kyr, Reid et al., 1996), supports a sediment supply insufficient to build a channelized fan turbidite system (Yose and Heller, 1989; Nelson et al., 1999). Such scattered distribution is observed along and at the base of the entire steep and rough slope (slope gradient up to 25°, Seibert et al., 2020) down to Guadeloupe, while southwards from Guadeloupe, the smoother

physiography shows well-identified single point sources, and associated distinct and long canyons and channels at their base (Seibert et al., 2020).

Additionally, the presence of a plunge pool associated with a slope-break deposit at the base of the slope in the Saint-Barthélémy (**Figure 11**) and Anguilla valleys (**Figure 10**) supports the occurrence of hydraulic jumps. Indeed, a slope-break deposit can be formed due to a significant change in slope gradient (Mulder and Alexander, 2001; Bourget et al., 2011; Migeon et al., 2012) close to a canyon mouth (Komar, 1971). The slope break that we observe ranges from 4° to 7°, and is consistent with other observations compatible with the formation of hydraulic jumps (Lee et al., 2002). One effect of hydraulic jumps is to disrupt the gravity flow, and thus maintain sediment in suspension and favor transport at the slope break (Gray et al., 2005). This process may contribute to lateral sediment dispersal towards distal sites and thus prevents a point source of sediment and channelization at the foot of the slope.

5.2 Types of Sediment Mixing

The sources of a turbidite system are a key control in their properties (Stow and Mayall, 2000). We identified two main types of sources: carbonate, due to the presence of the carbonate platforms, and siliciclastic, due to the erosion of the volcanic basement. In the study area, turbidite systems dominated by carbonate sediment overspill, are observed on the leeward edges of the shelves (Leeward Carbonate Slope—LCS; **Figures 3**, **13A,C**). From the shelf break to the deep basins, these systems extend from 65 to 130 km and are dominated by carbonate sediment overspill or direct sediment transfer from the shallow carbonate reefs through reef passes and gullies, such as on the northeastern slope of the Antigua Bank (**Figures 9A,E**). The Sombrero Escarpment is the only siliciclastic turbidite system, as it is mostly fed by the retrogressive erosion of the volcanic basement and volcaniclastic deposits (Sedimentary system 7, **Figures 13A,B**, **Table 2**). This sedimentary system is short (~20/30 km; **Table 2**) compared to the other systems in the study area. Finally, mixed systems (i.e., with carbonate and siliciclastic sources) are also identified in the study area. If two sediment sources settle in the same place, mixed systems can be defined at the "bed scale" (the mixing occurs within each bed), at the "lithofacies scale" (the mixing represents an alternation of beds for each lithology), or at "stratigraphic scale" (Chiarella et al., 2017).

In the study area, the two distinct sources are vertically arranged, since the carbonate source sits on top of the volcanic source, rather than "frontally arranged", with two distinct lateral lithologies (e.g., Cumberpatch et al., 2021). The mixed systems of this study are observable on the windward edges of the shelves (Sedimentary system 3, **Figure 13A**, **Table 2**). Indeed, these systems are fed by retrogressive erosion (**Figure 13D**) from both the platforms and shelf-edge (carbonate fraction) and the volcanic basement (volcanic fraction). This process is in accordance with other mixed systems as described offshore Australia (Puga-Bernabéu et al., 2011), where submarine canyons grow by retrogressive erosion after their initiation by a localized slope failure and/or sediment gravity flows. Depending on their stage of formation (juvenile stage with canyon on the lower slope, transitional stage on the middleslope, mature stage on the upper slope, Puga-Bernabéu et al., 2011), the nature of the dominant source varies, with dominance of the siliciclastic source (located on the slope) during young stages and a dominance of the carbonate source in the mature stages, when the canyon reaches the platform edge (canyons heads, **Figure 5A**). We, therefore, expect the mixing to occur mostly at a "bed-scale" (Chiarella et al., 2017), with both carbonate and siliciclastic sources mixed within each deposit. The proportion of each lithology should depend on the stage of formation of the canyon. We however anticipate a dominant carbonate fraction: low reflectivity in the Sombrero basin supports a limited siliciclastic delivery compared to in the carbonate valleys. We also expect some limited amount of mixing at the lithofacies scale, because of the presence of, either juvenile systems with canyons affecting solely the volcanic basement, or, slope failures.

5.3 Long-Term (Kyr to Myr) Controls on Sediment Transfer

5.3.1 Glacio-Eustatism

Some features of the NLAS support the importance of eustatism on carbonate sediment productivity and transfer: A) drowned reefs or platforms on the Anguilla Bank indicate past periods of exposure and/or drowning of the platform (Schlager, 1989, 1998; Leclerc et al., 2014; Leclerc and Feuillet, 2019; Carey et al., 2020), and B) unconformities between seismic units in the Anguilla Valley (**Figures 10C,D**) and the St-Barthélémy Valley (**Figure 7B**) highlight periods with variation in sediment transport.

In tropical carbonate turbidite systems, eustatic fluctuations have generally a high impact on sedimentation (Dunbar and Dickens, 2003; Tcherepanov et al., 2008). During sea-level highstands, carbonate productivity is usually enhanced (Reijmer et al., 1988; Schlager et al., 1994; Chabaud et al., 2016), providing high amounts of bioclasts and carbonate muds available for sediment transport. Conversely, during sea-level lowstands, production and off-bank transport are generally reduced while cementation, lithification, and induration of shallow-water carbonates are increased (Schlager et al., 1994; Chabaud et al., 2016), and thus prevent remobilization by currents and waves. Moreover, dissolution rather than erosion of carbonates prevails onshore (Chabaud et al., 2016), furthermore reducing sediment input during lowstands. Limited deposition of gravity flows may however also occur during lowstands, mainly at proximal locations of turbidite systems as documented for the Glorieuses islands (Jorry et al., 2020) and supported by higher seafloor reflectivity, suggesting some reworking on the upper slope.

Carbonate systems of the NLAS are therefore most likely active during sea-level highstands and less active during sea-level lowstands, such as in other mixed systems (Schlager et al., 1994; Jorry et al., 2008; McArthur et al., 2013). In contrast, the top of the siliciclastic system is too deep (~900 mbsl) to be influenced by glacio-eustatic sea-level fluctuations as usually observed in

siliciclastic systems, which are more active during sea-level lowstands (Posamentier et al., 1991; Vail et al., 1991; Hübscher et al., 1997).

5.3.2 Tectonics

Tectonics can play an important role in sediment transfer and destabilization, particularly along active margins, where vertical motions can deflect or dam transfer axis, modify the availability of sediment supply or drive the failure of over-steepened slopes (Laursen and Normark, 2002; Mountjoy et al., 2009; Michaud et al., 2011; Ratzov et al., 2012; Collot et al., 2019; Seibert et al., 2020; Claussmann et al., 2021a). Subsidence outlined by the presence of two tilted carbonate paleo-platforms at 700 mbsl and 1,600 mbsl (**Figure 8**) is consistent with the drastic subsidence of the forearc identified by Boucard et al., 2021. The present-day relatively deep position of these features, which were formed at a very shallow depth, attests to the important role of subsidence, probably accentuated along the Tintamarre Spur. For instance, at Les Saintes (offshore Guadeloupe), the subsidence of the Quaternary coral reef (Leclerc et al., 2014) is estimated at a rate of -0.3 to −0.45 mm/yr since the late Pleistocene (Leclerc and Feuillet, 2019), while in the north, this estimation reaches 340 m/Myr (0.34 mm/yr) in the deepest outer forearc since middle Miocene (Boucard et al., 2021). Possible causes of subsidence are debated, but include: A) a thermal origin caused by the cooling of the lithosphere related to a decline in volcanic activity and westward migration of the volcanic arc since the Miocene (Bouysse and Westercamp, 1990; Legendre et al., 2018); B) regional subsidence of the arc due to long-term plate motion along the subduction megathrust over several seismic cycles (Leclerc and Feuillet, 2019); or C) basal erosion of the upper plate by over pressured fluids related to a fully-hydrated subduction zone (Paulatto et al., 2017; Marcaillou et al., 2021).

Independently of the causes of tectonics in the area, two general effects are directly induced. The first is the opening of V-shaped valleys in map view (*sensu* Boucard et al., 2021), which created a complex morphology departing from a classical circular or elongated shape of the banks and shelf-edges; this promotes multiple edges that are either windward or leeward oriented, thus favoring, or not, carbonate transport off-bank. The second is the over-steepening of valley walls (or spurs, or flanks) bounded by normal faults. This last effect directly influences slope stability, the amount of retrogressive erosion, sediment production, and the formation of plunge pools due to hydraulic jumps. Indeed, the stability of plunge pools over time; demonstrated by the presence of a buried and tilted plunge pool along with unconformity U4, would have involved a slope-break angle of a few degrees to allow for a hydraulic jump (Komar, 1971). This break is probably maintained by fault activity, preventing sediment accumulation and progressive flattening at the foot of the slope (Bourget et al., 2011). The two combined effects of tectonics thus account for the long-term lack of point sources, scattered sediment delivery, and the mixing of the system.

5.3.3 Seismicity

The main particularity of the NLAS is the proximity of a subduction zone, implying possible seismically-triggered gravity-driven currents (see for example Goldfinger et al., 2003; Ratzov et al., 2015). In at least seven separate forearc sub-basins, thick transparent units (megabeds) are visible in sub-bottom profiles (**Figure 12**) and could correspond to homogenites or megaturbidites. Similar deposits are explained in the literature as resulting from surficial sediment remobilization (McHugh et al., 2016; McHugh et al., 2020), or from a seiche effect induced by seismic waves in a confined basin or in a lake (Chapron et al., 1999; Beck et al., 2007). Alternative explanations include the waning flow of a turbidity current triggered by an earthquake (Polonia et al., 2017) or the resuspension of shallow sediment due to a tsunami (San Pedro et al., 2017). The identification of MTDs (**Figures 7A**, **12D,H**), which can be triggered by earthquakes (Moscardelli and Wood, 2016 and reference therein), confirms that seismicity is an important parameter considering sediment transfer in the study area. Ongoing detailed chronostratigraphy and dating of these deposits (Morena, 2020) should define the timing and spatial correlation across the margin, to infer a regional trigger, most likely caused by an earthquake as documented by Goldfinger et al. (2003).

6 CONCLUSION

The study of modern depositional sedimentary systems, especially concerning multi-sources (siliciclastic, carbonate, or mixed) sedimentary systems has significantly progressed over the last decade (e.g., Chiarella et al., 2017), even if the coexistence of adjacent systems of distinctive nature is scarcely documented. In the Northern Lesser Antilles Segment, carbonate and siliciclastic sources coexist within 150 km on two wide and shallow carbonate shelves (carbonate sources) and a steep insular and mainly volcanic slope (siliciclastic source). Morphological factors, such as the slope gradient or the orientation of the shelf edge with respect to wind and current, are determining factors for the nature of the source:

- Siliciclastic sedimentary systems are disconnected by a morphological dam from the main carbonate platforms or sources and are likely fed by retrogressive erosion of the steep volcanic slopes
- Carbonate sedimentary systems are sourced from the leeward edges of the carbonate platforms by carbonate overspill through numerous small, narrow canyons originating at the shelf edge
- Mixed sedimentary systems are identified on the windward edges of carbonate platforms incised by slope-confined canyons through retrogressive- and downward-cutting erosion

Tectonic activity plays a major role in the coexistence of adjacent distinctive sedimentary systems, since the normal

faults created a complex morphology dominated by V-shaped valleys in map view, which offer an alternation of leeward, and windward edges favoring carbonate- or mixed-systems. Additionally, the steep slope gradient induced by normal faults and tilting seems to be the main factor controlling sediment dispersal, for example by causing multiple line sources, and the dispersion of gravity-driven currents under the effect of hydraulic jump in areas of marked slope break. Evidence of paleo-platforms in the Tintamarre Spur and unconformities in the valleys also support the importance of tectonics in the area for all the sedimentary systems, while drowned platforms might imply the strong influence of glacio-eustatism on the carbonate system. Ongoing marine paleoseismic studies could allow us to verify the role of seismicity as a triggering-factor for slope destabilizations leading to the occurrence of gravity-driven currents and their deposit in the forearc basin.

Our study provides a modern analog of adjacent systems dominated by distinctive lithologies in a tectonically active area. The results appear particularly appropriate to decipher the nature of ancient source-to-sink systems dominated by complex tectonics, paleo-bathymetry, and sediment routings.

DATA AVAILABILITY STATEMENT

The original contributions presented in the study are included in the article and **Supplementary Material**; further inquiries can be directed to the corresponding author or to SISMER. The DOIs of the oceanographic cruises are: https://doi.org/10.17600/16001800 for ANTITHESIS 1 cruise, doi: 10.17600/13010070 for ANTITHESIS 3 cruise and doi: 10.17600/16001700 for CASEIS cruise.

AUTHOR CONTRIBUTIONS

PM was involved in all the stages of the production of the study, including data analysis, figures realization and writing of the paper. GR was involved in the data acquisition and was involved in all the stages of the production of the study. AC was involved in all the stages of the production of the manuscript. FK was involved in the production of the manuscript and was co-Principal Investigator of the ANTITHESIS cruises. CB was involved in the data acquisition and was involved in the final reading of the manuscript. CS was involved in the data acquisition and processing, and was involved in the final reading of the manuscript. BM was the Principal Investigator of the ANTITHESIS cruises and was involved in the data acquisition and in the final reading of the manuscript. NF was the Principal Investigator of the CASEIS cruise, was involved in the data acquisition and in the final reading of the manuscript.

ACKNOWLEDGMENTS

The authors thank the Captain, crew, and scientific team of CASEIS cruise (DOI:10.17600/16001800) and ANTITHESIS cruises (DOI: 10.17600/13010070). This study was accomplished within the framework of the French ANR CARQUAKES project, contract number ANR-17-CE3-0006, the LABEX UnivEearthS project WP2.1, the PREST intereg Caraïbe project, the BQR IPGP, the CNRS-INSU, the BQR Observatoire Côte d'Azur, and the Université Côte d'Azur (CSI 2016-DR-066). The PhD of Pierre Morena was funded by IFREMER and Région Bretagne. The authors thank Alison Chalm (Ifremer, Brest) for her efficiency in the English correction of the manuscript. The authors also thank Sébastien Migeon (Geoazur, Valbonne) for scientific discussions. The authors thank Jenny Trévisan (Geoazur, Valbonne) for DEM processing; Frédérique Leclerc (Geoazur, Valbonne), Muriel Laurencin (UBO, Brest), Jean-Marie Saurel (IPGP, Paris), Gaëlle Bénâtre (IPGP, Paris), and Eric Jacques (IPG, Paris) for MCS data processing; and Hervé Bisquay and Laurence Morvan (Genavir, Brest) for multibeam data processing. The authors finally thank Barbara Claussmann (Schlumberger, United Kingdom), Lesli Wood (Colorado School of Mines, United States) and Adam McArthur (University of Leeds, United Kingdom) for their constructive review, as well as Ángel Puga-Bernabéu (University of Granada, Spain) for his comments on an early version of the manuscript.

SUPPLEMENTARY MATERIAL

The Supplementary Material for this article can be found online at: https://www.frontiersin.org/articles/10.3389/feart.2022.834029/full#supplementary-material

REFERENCES

Andréïeff, P., Baubron, J. C., and Westercamp, D. (1988a). Histoire géologique de la Martinique (Petites Antilles): biostratigraphie (foraminifères), radiochronologie (potassium–argon), évolution volcano-structurale. *Géologie Fr.* 2-3, 39–70.

Andréïeff, P., Westercamp, D., Garrabé, F., and Bonneton, J. R. (1988b). Stratigraphie de l'île de Saint-Martin. *Géologie Fr.* 2-3, 71–88.

Bailleul, J., Robin, C., Chanier, F., Guillocheau, F., Field, B., and Ferriere, J. (2007). Turbidite Systems in the Inner Forearc Domain of the Hikurangi Convergent Margin (New Zealand): New Constraints on the Development of Trench-Slope Basins. *J. Sediment. Res.* 77 (4), 263–283. doi:10.2110/jsr.2007.028

Beck, C. (2009). "Late Quaternary Lacustrine Paleo-Seismic Archives in North-Western Alps: Examples of Earthquake-Origin Assessment of Sedimentary Disturbances". *Earth-Science Rev.* 96, 327–344. doi:10.1016/j.earscirev.2009.07.005

Beck, C., Mercier de Lepinay, B., Schneider, J.-L., Cremer, M., Cağatay, N., Wendenbaum, E., et al. (2007). Late Quaternary Co-seismic Sedimentation in the Sea of Marmara's Deep Basins. *Sediment. Geol.* 199 (1-2), 65–89. doi:10.1016/j.sedgeo.2005.12.031

Beck, C., Reyss, J.-L., Leclerc, F., Moreno, E., Feuillet, N., Barrier, L., et al. (2012). Identification of Deep Subaqueous Co-seismic Scarps through Specific Coeval Sedimentation in Lesser Antilles: Implication for Seismic Hazard. *Nat. Hazards Earth Syst. Sci. Eur. Geosciences Union* 12, 1–13. doi:10.5194/nhess-12-1755-2012

Benâtre, G., Feuillet, N., Carton, H., Jacques, E., and Pichot, T. (2020). *Main Active Structures in the Barbados Accretionary Wedge of the Lesser Antilles Subduction: Implications for Slip Partitioning*. Vienna: EGU Fall Meeting.

Bertran, P., Bonnissent, D., Imbert, D., Lozouet, P., Serrand, N., and Stouvenot, C. (2004). Paléoclimat des Petites Antilles depuis 4000 ans BP : l'enregistrement de la lagune de Grand-Case à Saint-Martin. *Comptes Rendus Geosci.* 336 (16), 1501–1510. doi:10.1016/j.crte.2004.09.009

Boucard, M., Marcaillou, B., Lebrun, J. F., Laurencin, M., Klingelhoefer, F., Laigle, M., et al. (2021). Paleogene V-Shaped Basins and Neogene Subsidence of the Northern Lesser Antilles Forearc. *Tectonics* 40, e2020TC006524. doi:10.1029/2020TC006524

Bourget, J., Zaragosi, S., Ellouz-zimmermann, N., Mouchot, N., Garlan, T., Schneider, J.-L., et al. (2011). Turbidite System Architecture and Sedimentary Processes along Topographically Complex Slopes: the Makran Convergent Margin. *Sedimentology* 58 (2), 376–406. doi:10.1111/j.1365-3091.2010.01168.x

Bouysse, P., Andréïeff, P., Richard, M., Baubron, J. C., Mascle, A., Maury, R. C., et al. (1985). "Aves Swell and Northern Lesser Antilles Ridge: Rock-Dredging Results from ARCANTE 3 Cruise," in *Géodynamique des Caraibes, Symposium* (Paris: Editions Technip), 65–76.

Bouysse, P., and Guennoc, P. (1983). Données sur la structure de l'arc insulaire des petites antilles, entre Ste-Lucie et Anguilla. *Mar. Geol.* 53 (1-2), 131–166. doi:10.1016/0025-3227(83)90038-5

Bouysse, P., and Westercamp, D. (1990). Subduction of Atlantic Aseismic Ridges and Late Cenozoic Evolution of the Lesser Antilles Island Arc. *Tectonophysics* 175 (4), 349–380. doi:10.1016/0040-1951(90)90180-g

Braga, J. C., Martin, J. M., and Wood, J. L. (2001). Submarine Lobes and Feeder Channels of Redeposited, Temperate Carbonate and Mixed Siliciclastic-Carbonate Platform Deposits (Vera Basin, Almería, Southern Spain). *Sedimentology* 48, 99–116. doi:10.1046/j.1365-3091.2001.00353.x

Briden, J. C., Rex, D. C., Faller, A. M., and Tomblin, J. F. (1979). K-ar Geochronology and Palaeomagnetism of Volcanic Rocks in the Lesser Antilles Island Arc. *Philosophical Trans. R. Soc. B Biol. Sci.* 291, 485–528. doi:10.1098/rsta.1979.0040

Brink, U. t., Danforth, W., Polloni, C., Andrews, B., Llanes, P., Smith, S., et al. (2004). New Seafloor Map of the Puerto Rico Trench Helps Assess Earthquake and Tsunami Hazards. *Eos Trans. AGU* 85 (Issue 37), 349–354. doi:10.1029/2004EO370001

Budd, A. F., Johnson, K. G., and Edwards, J. C. (1995). Caribbean Reef Coral Diversity during the Early to Middle Miocene: An Example from the Anguilla Formation. *Coral Reefs* 14, 109–117. doi:10.1007/bf00303432

Carey, S., Sparks, R. S. J., Tucker, M. E., Li, T., Robinson, L., Watt, S. F. L., et al. (2020). The Polygenetic Kahouanne Seamounts in the Northern Lesser Antilles Island Arc: Evidence for Large-Scale Volcanic Island Subsidence. *Mar. Geol.* 419, 106046. doi:10.1016/j.margeo.2019.106046

Chabaud, L., Ducassou, E., Tournadour, E., Mulder, T., Reijmer, J. J. G., Conesa, G., et al. (2016). Sedimentary Processes Determining the Modern Carbonate Periplatform Drift of Little Bahama Bank. *Mar. Geol.* 378, 213–229. doi:10.1016/j.margeo.2015.11.006

Chapron, E., Beck, C., Pourchet, M., and Deconinck, J-F. (1999). 1822 Earthquake-Triggered Homogenite in Lake Le Bourget (NW Alps). *Terra nova.* 11 (2-3), 86–92. doi:10.1046/j.1365-3121.1999.00230.x

Chiarella, D., Longhitano, S. G., and Tropeano, M. (2019). Different Stacking Patterns along an Active Fold-And-Thrust Belt-Acerenza Bay, Southern Apennines (Italy). *Geology* 47 (2), 139–142. doi:10.1130/g45628.1

Chiarella, D., Longhitano, S. G., and Tropeano, M. (2017). Types of Mixing and Heterogeneities in Siliciclastic-Carbonate Sediments. *Mar. Petroleum Geol.* 88, 617–627. doi:10.1016/j.marpetgeo.2017.09.010

Christeson, G. L., Mann, P., Escalona, A., and Aitken, T. J. (2008). Crustal Structure of the Caribbean–Northeastern South America Arc-Continent Collision Zone. *J. Geophys. Res.* 113, 1–19. doi:10.1029/2007jb005373

Christman, R. A. (1953). Geology of St. Bartholomew, St. Martin and Anguilla, Lesser Antilles. *Geol. Soc. Am. Bull.* 64 (1), 65–96. doi:10.1130/0016-7606(1953)64[85:gosbsm]2.0.co;2

Claussmann, B., Bailleul, J., Chanier, F., Caron, V., Mcarthur, A. D., Mahieux, G., et al. (2021b). Contrasting Mixed Siliciclastic-Carbonate Shelf-Derived Gravity-Driven Systems in Compressional Intra-slope Basins (Southern Hikurangi Margin, New Zealand). *Mar. Petroleum Geol.* 134, 105252. doi:10.1016/j.marpetgeo.2021.105252

Claussmann, B., Bailleul, J., Chanier, F., Mahieux, G., Caron, V., Mcarthur, A. D., et al. (2021a). Shelf-derived Mass-Transport Deposits: Origin and Significance in the Stratigraphic Development of Trench-Slope Basins. *N. Z. J. Geol. Geophys.* 65 (1), 17–52. doi:10.1080/00288306.2021.1918729

Collot, J. Y., Ratzov, G., Silva, P., Proust, J. N., Migeon, S., Hernandez, M. J., et al. (2019). The Esmeraldas Canyon: A Helpful Marker of the Pliocene-Pleistocene Tectonic Deformation of the North Ecuador-Southwest Colombia Convergent Margin. *Tectonics* 38, 3140–3166. doi:10.1029/2019TC005501

Cornée, J.-J., Léticée, J.-L., Münch, P., Quillévéré, F., Lebrun, J.-F., Moissette, P., et al. (2012). Sedimentology, Palaeoenvironments and Biostratigraphy of the Pliocene-Pleistocene Carbonate Platform of Grande-Terre (Guadeloupe, Lesser Antilles Forearc). *Sedimentology* 59, 1426–1451. doi:10.1111/j.1365-3091.2011.01311.x

Cornee, J. J., Münch, P., Philippon, M., Boudagher-Fadel, M., Quillévéré, F., Melinte-Dobrinescu, M., et al. (2021). Lost Islands in the Northern Lesser Antilles: Possible Milestones in the Cenozoic Dispersal of Terrestrial Organisms between South-America and the Greater Antilles. *Earth-Science Rev.* 2021, 103617. doi:10.1016/j.earscirev.2021.103617

Ćosović, V., Mrinjek, E., Nemec, W., Španiček, J., and Terzić, K. (2018). Development of Transient Carbonate Ramps in an Evolving Foreland Basin. *Basin Res.* 30 (4), 746–765.

Counts, J. W., Jorry, S. J., Leroux, E., Miramontes, E., and Jouet, G. (2018). Sedimentation Adjacent to Atolls and Volcano-Cored Carbonate Platforms in the Mozambique Channel (SW Indian Ocean). *Mar. Geol.* 404, 41–59. doi:10.1016/j.margeo.2018.07.003

Cumberpatch, Z. A., Soutter, E. L., Kane, I. A., Casson, M., and Vincent, S. J. (2021). Evolution of a Mixed Siliciclastic-carbonate Deep-marine System on an Unstable Margin: The Cretaceous of the Eastern Greater Caucasus, Azerbaijan. *Basin Res.* 33 (1), 612–647. doi:10.1111/bre.12488

DeMets, C., Gordon, R. G., and Argus, D. F. (2010). Geologically Current Plate Motions. *Geophys. J. Int.* 181, 1–80. doi:10.1111/j.1365-246X.2009.04491.x

Deville, E., Mascle, A., Callec, Y., Huyghe, P., Lallemant, S., Lerat, O., et al. (2015). Tectonics and Sedimentation Interactions in the East Caribbean Subduction Zone: An Overview from the Orinoco Delta and the Barbados Accretionary Prism. *Mar. Petroleum Geol.* 64, 76–103. doi:10.1016/j.marpetgeo.2014.12.015

Dorsey, R. J., and Kidwell, S. M. (1999). Mixed Carbonate-Siliciclastic Sedimentation on a Tectonically Active Margin: Example from the Pliocene of Baja California Sur, Mexico. *Geol* 27 (10), 935–938. doi:10.1130/0091-7613(1999)027<0935:mcssoa>2.3.co;2

Droxler, A. W., and Schlager, W. (1985). Glacial versus Interglacial Sedimentation Rates and Turbidite Frequency in the Bahamas. *Geol* 13 (11), 799–802. doi:10.1130/0091-7613(1985)13<799:gvisra>2.0.co;2

Dunbar, G. B., and Dickens, G. R. (2003). Late Quaternary Shedding of Shallow-Marine Carbonate along a Tropical Mixed Siliciclastic-Carbonate Shelf: Great Barrier Reef, Australia. *Sedimentology* 50 (6), 1061–1077. doi:10.1046/j.1365-3091.2003.00593.x

Eberli, G. P., and Ginsburg, R. N. (1987). Segmentation and Coalescence of Cenozoic Carbonate Platforms, Northwestern Great Bahama Bank. *Geol* 15 (1), 75–79. doi:10.1130/0091-7613(1987)15<75:sacocc>2.0.co;2

Fauquembergue, K., Ducassou, E., Mulder, T., Hanquiez, V., Perello, M.-C., Poli, E., et al. (2018). Genesis and Growth of a Carbonate Holocene Wedge on the Northern Little Bahama Bank. *Mar. Petroleum Geol.* 96, 602–614. doi:10.1016/j.marpetgeo.2018.05.013

Feuillet, N., Beauducel, F., and Tapponnier, P. (2011). Tectonic Context of Moderate to Large Historical Earthquakes in the Lesser Antilles and Mechanical Coupling with Volcanoes. *J. Geophys. Res.* 116, B10. doi:10.1029/2011JB008443

Feuillet, N. (2016). CASEIS Cruise, RV Pourquoi Pas ? https://campagnes.flotteoceanographique.fr/campagnes/16001800/. doi:10.17600/16001800

Feuillet, N., Leclerc, F., Tapponnier, P., Beauducel, F., Boudon, G., Le Friant, A., et al. (2010). Active Faulting Induced by Slip Partitioning in Montserrat and Link with Volcanic Activity: New Insights from the 2009 GWADASEIS Marine Cruise Data. *Geophys. Res. Lett.* 37, 19. doi:10.1029/2010gl042556

Feuillet, N., Manighetti, I., Tapponnier, P., and Jacques, E. (2002). Arc Parallel Extension and Localization of Volcanic Complexes in Guadeloupe, Lesser Antilles. *J. Geophys. Res.* 107 (B12), 3–1. doi:10.1029/2001JB000308

Feuillet, N., Tapponnier, P., Manighetti, I., Villemant, B., and King, G. C. P. (2004). Differential Uplift and Tilt of Pleistocene Reef Platforms and Quaternary Slip

Rate on the Morne-Piton Normal Fault (Guadeloupe, French West Indies). *J. Geophys. Res. Solid Earth* 109, B2. doi:10.1029/2003jb002496

Goldfinger, C., Nelson, H. C., and Johnson, J. E. (2003). Shipboard Scientific PartyDeep-Water Turbidites as Holocene Earthquake Proxies: the Cascadia Subduction Zone and Northern San Andreas Fault Systems. *Ann. Geophys.* 46 (5), 1169–1194.

Gonzalez, R., and Eberli, G. P. (1997). Sediment Transport and Bedforms in a Carbonate Tidal Inlet; Lee Stocking Island, Exumas, Bahamas. *Sedimentology* 44 (6), 1015–1030. doi:10.1046/j.1365-3091.1997.d01-59.x

Gray, T. E., Alexander, J., and Leeder, M. R. (2005). Quantifying Velocity and Turbulence Structure in Depositing Sustained Turbidity Currents across Breaks in Slope. *Sedimentology* 52 (3), 467–488. doi:10.1111/j.1365-3091.2005.00705.x

Haak, A. B., and Schlager, W. (1989). Compositional Variations in Calciturbidites Due to Sea-Level Fluctuations, Late Quaternary, Bahamas. *Geol. Rundsch* 78 (2), 477–486. doi:10.1007/bf01776186

Hans Nelson, C., Karabanov, E. B., Colman, S. M., and Escutia, C. (1999). Tectonic and Sediment Supply Control of Deep Rift Lake Turbidite Systems: Lake Baikal, Russia. *Geol* 27 (2), 163–166. doi:10.1130/0091-7613(1999)027<0163:tassco>2.3.co;2

Hassoun, V., Migeon, S., Cattaneo, A., Larroque, C., and Mercier de Lepinay, B. (2009). "Imbricated Scars on the Ligurian Continental Slope: Evidence for Multiple Failure Events in the 1887 Eathquake Epicentral Area," in International Conference on Seafloor Mapping for Geohazard Assessment, Ischia, Italy, May 11–13, 2009 (World Academy of Science, Engineering and Technology), 7, 11–13.

Hübscher, C., Spieβ, V., Breizke, M., and Weber, M. E. (1997). The Youngest Channel-Levee System of the Bengal Fan: Results from Digital Sediment Echosounder Data. *Mar. Geol.* 141, 125–145.

Iacono, C. L., Gràcia, E., Diez, S., Bozzano, G., Moreno, X., Dañobeitia, J., et al. (2008). Seafloor Characterization and Backscatter Variability of the Almería Margin (Alboran Sea, SW Mediterranean) Based on High-Resolution Acoustic Data. *Mar. Geol.* 250 (1-2), 1–18. doi:10.1016/j.margeo.2007.11.004

Jany, I., Scanlon, K. M., and Mauffret, A. (1990). Geological Interpretation of Combined Seabeam, Gloria and Seismic Data from Anegada Passage (Virgin Islands, North Caribbean). *Mar. Geophys Res.* 12 (3), 173–196. doi:10.1007/bf02266712

Jorry, S. J., Camoin, G. F., Jouet, G., Roy, P. L., Vella, C., Courgeon, S., et al. (2016). Modern Sediments and Pleistocene Reefs from Isolated Carbonate Platforms (Iles Eparses, SW Indian Ocean): a Preliminary Study. *Acta Oecol.* 72, 129–143. doi:10.1016/j.actao.2015.10.014

Jorry, S. J., Droxler, A. W., Mallarino, G., Dickens, G. R., Bentley, S. J., Beaufort, L., et al. (2008). Bundled Turbidite Deposition in the Central Pandora Trough (Gulf of Papua) since Last Glacial Maximum: Linking Sediment Nature and Accumulation to Sea Level Fluctuations at Millennial Timescale. *J. Geophys. Res.* 113. doi:10.1029/2006JF000649

Jorry, S. J., Jouet, G., Edinger, E. N., Toucanne, S., Counts, J. W., Courgeon, S., et al. (2020). From Platform Top to Adjacent Deep Sea: New Source-to-Sink Insights into Carbonate Sediment Production and Transfer in the SW Indian Ocean (Glorieuses archipelago).. *Marine Geology* 423, 106144. doi:10.1016/j.margeo.2020.106144

Kastens, K. A., and Cita, M. B. (1981). Tsunami-induced Sediment Transport in the Abyssal Mediterranean Sea. *Geol. Soc. Am. Bull.* 92 (11), 845–857. doi:10.1130/0016-7606(1981)92<845:tstita>2.0.co;2

Komar, P. D. (1971). Hydraulic Jumps in Turbidity Currents. *Geol. Soc. Am. Bull.* 82 (6), 1477–1488. doi:10.1130/0016-7606(1971)82[1477:hjitc]2.0.co;2

Kopp, H., Weinzierl, W., Becel, A., Charvis, P., Evain, M., Flueh, E. R., et al. (2011). Deep Structure of the Central Lesser Antilles Island Arc: Relevance for the Formation of Continental Crust. *Earth Planet. Sci. Lett.* 304, 121–134. doi:10.1016/j.epsl.2011.01.024

Laban, C., Cameron, T. D. J., and Schüttenhelm, R. T. E. (1984). Geologie van het Kwartair in de zuidelijke bocht van de Noordzee. *Meded. Werkgr. Tert. Kwartaire Geol.* 21 (3), 139–153.

Laurencin, M. (2017). *Etude de la géométrie, de la nature et des déformations de la zone de subduction des Petites Antilles du Nord*. Brest: University of Bretagne Loire, 294. PhD Thesis.

Laurencin, M., Graindorge, D., Klingelhoefer, F., Marcaillou, B., and Evain, M. (2018). Influence of Increasing Convergence Obliquity and Shallow Slab Geometry onto Tectonic Deformation and Seismogenic Behavior along the Northern Lesser Antilles Zone. *Earth Planet. Sci. Lett.* 492, 59–72. doi:10.1016/j.epsl.2018.03.048

Laurencin, M., Marcaillou, B., Graindorge, D., Klingelhoefer, F., Lallemand, S., Laigle, M., et al. (2017). The Polyphased Tectonic Evolution of the Anegada Passage in the Northern Lesser Antilles Subduction Zone. *Tectonics* 36 (5), 945–961. doi:10.1002/2017TC004511

Laurencin, M., Marcaillou, B., Graindorge, D., Lebrun, J. F., Klingelhoefer, F., Boucard, M., et al. (2019). The Bunce Fault and Strain Partitioning in the Northern Lesser Antilles. *Geophys. Res. Lett.* 46, 9573–9582. doi:10.1029/2019GL083490

Laursen, J., and Normark, W. R. (2002). Late Quaternary Evolution of the San Antonio Submarine Canyon in the Central Chile Forearc (33°S). *Mar. Geol.* 188 (3-4), 365–390. PII:S0025-3227(02)00421-8. doi:10.1016/s0025-3227(02)00421-8

Leclerc, F., Feuillet, N., Cabioch, G., Deplus, C., Lebrun, J. F., Bazin, S., et al. (2014). The Holocene Drowned Reef of Les Saintes Plateau as Witness of a Long-Term Tectonic Subsidence along the Lesser Antilles Volcanic Arc in Guadeloupe. *Mar. Geol.* 355, 115–135. doi:10.1016/j.margeo.2014.05.017

Leclerc, F., and Feuillet, N. (2019). Quaternary Coral Reef Complexes as Powerful Markers of Long-Term Subsidence Related to Deep Processes at Subduction Zones: Insights from Les Saintes (Guadeloupe, French West Indies). *Geosphere* 15 (4), 983–1007. doi:10.1130/GES02069.1

Lee, S. E., Talling, P. J., Ernst, G. G. J., and Hogg, A. J. (2002). Occurrence and Origin of Submarine Plunge Pools at the Base of the US Continental Slope. *Mar. Geol.* 185 (3-4), 363–377. PII:S0025-3227(01)00298–5. doi:10.1016/s0025-3227(01)00298-5

Legendre, L., Philippon, M., Münch, P., Leticée, J. L., Noury, M., Maincent, G., et al. (2018). Trench Bending Initiation: Upper Plate Strain Pattern and Volcanism. Insights from the Lesser Antilles Arc, St. Barthelemy Island, French West Indies. *Tectonics* 37 (9), 2777–2797. doi:10.1029/2017TC004921

Malaizé, B., Bertran, P., Carbonel, P., Bonnissent, D., Charlier, K., Galop, D., et al. (2011). Hurricanes and Climate in the Caribbean during the Past 3700 Years BP. *Holocene* 21 (6), 911–924. doi:10.1177/0959683611400198

Mann, P., Prentice, C. S., Hippolyte, J.-C., Grindlay, N. R., Abrams, L. J., and Lao´-Da´vila, D. (2005). "Reconnaissance Study of Late Quaternary Faulting along Cerro Goden Fault Zone, Western Puerto Rico," in *Active Tectonics an Seismic Hazards of Puerto Rico, the Virgin Islands and Off-Shore Areas*. Editor P. Mann (America: Geological Society of America), 115–138. doi:10.1130/0-8137-2385-x.115

Marcaillou, B., and Klingelhoefer, F. (2013). *ANTITHESIS-1-Leg1 Cruise*. RV L'Atalante. doi:10.17600/13010070

Marcaillou, B., and Klingelhoefer, F. (2016). *ANTITHESIS-3 Cruise*. RV Pourquoi Pas? doi:10.17600/16001700

Marcaillou, B., Klingelhoefer, F., Laurencin, M., Lebrun, J.-F., Laigle, M., Lallemand, S., et al. (2021). Pervasive Detachment Faults within the Slow Spreading Oceanic Crust at the Poorly Coupled Antilles Subduction Zone. *Commun. Earth Environ.* 2. doi:10.1038/s43247-021-00269-6

Mascle, A., and Westercamp, D. (1983). Geologie d'Antigua, Petites Antilles. *Bull. Société géologique Fr.* S7-XXV, 855–866. doi:10.2113/gssgfbull.s7-xxv.6.855

McArthur, A. D., Hartley, A. J., and Jolley, D. W. (2013). Stratigraphic Development of an Upper Jurassic Deep Marine Syn-Rift Succession, Inner Moray Firth Basin, Scotland. *Basin Res.* 25 (3), 285–309. doi:10.1111/j.1365-2117.2012.00557.x

McHugh, C. M., Kanamatsu, T., Seeber, L., Bopp, R., Cormier, M.-H., and Usami, K. (2016). Remobilization of Surficial Slope Sediment Triggered by the A.D. 2011 Mw9 Tohoku-Oki Earthquake and Tsunami along the Japan Trench. *Geology* 44, 391–394. doi:10.1130/G37650.1

McHugh, C. M., Seeber, L., Rasbury, T., Strasser, M., Kioka, A., Kanamatsu, T., et al. (2020). Isotopic and Sedimentary Signature of Megathrust Ruptures along the Japan Subduction Margin. *Mar. Geol.* 428, 106283. doi:10.1016/j.margeo.2020.106283

Michaud, F., Calmus, T., Ratzov, G., Royer, J. Y., Sosson, M., Bigot-Cormier, F., et al. (2011). Active Deformation along the Southern End of the Tosco-Abreojos Fault System: New Insights from Multibeam Swath Bathymetry. *Pure Appl. Geophys.* 168 (8), 1363–1372. doi:10.1007/s00024-010-0193-y

Migeon, S., Mulder, T., Savoye, B., and Sage, F. (2012). Hydrodynamic Processes, Velocity Structure and Stratification in Natural Turbidity Currents: Results

Inferred from Field Data in the Var Turbidite System. *Sediment. Geol.* 245-246, 48–62. doi:10.1016/j.sedgeo.2011.12.007

Morena, P. (2020). *Paléosismologie et potentiel sismogène de la zone de subduction des Petites Antilles à partir de l'enregistrement sédimentaire*. Brest: University of Bretagne Occidentale, 340. PhD Thesis.

Moscardelli, L., Ochoa, J., Hunt, I., and Zahm, L. (2019). Mixed Siliciclastic-Carbonate Systems and Their Impact for the Development of Deep-Water Turbidites in Continental Margins: A Case Study from the Late Jurassic to Early Cretaceous Shelburne Subbasin in Offshore Nova Scotia. *Bulletin* 103 (10), 2487–2520. doi:10.1306/02151917318

Moscardelli, L., and Wood, L. (2016). Morphometry of Mass-Transport Deposits as a Predictive Tool. *Bulletin* 128 (1-2), 47–80.

Mountjoy, J. J., Barnes, P. M., and Pettinga, J. R. (2009). Morphostructure and Evolution of Submarine Canyons across an Active Margin: Cook Strait Sector of the Hikurangi Margin, New Zealand. *Mar. Geol.* 260 (1-4), 45–68. doi:10.1016/j.margeo.2009.01.006

Mulder, T., and Alexander, J. (2001). Abrupt Change in Slope Causes Variation in the Deposit Thickness of Concentrated Particles-Driven Density Currents. *Mar. Geol.* 175 (1-4), 221–235. PII: S0025-3227(01)001 14-1. doi:10.1016/s0025-3227(01)00114-1

Mulder, T., Ducassou, E., Eberli, G. P., Hanquiez, V., Gonthier, E., Kindler, P., et al. (2012a). New Insights into the Morphology and Sedimentary Processes along the Western Slope of Great Bahama Bank. *Geology* 40 (7), 603–606. doi:10.1130/G32972.1

Mulder, T., Ducassou, E., Gillet, H., Hanquiez, V., Tournadour, E., Combes, J., et al. (2012b). Canyon Morphology on a Modern Carbonate Slope of the Bahamas: Evidence of Regional Tectonic Tilting. *Geology* 40 (9), 771–774. doi:10.1130/G33327.1

Mulder, T., Joumes, M., Hanquiez, V., Gillet, H., Reijmer, J. J. G., Tournadour, E., et al. (2017). Carbonate Slope Morphology Revealing Sediment Transfer from Bank-To-Slope (Little Bahama Bank, Bahamas). *Mar. Petroleum Geol.* 83, 26–34. doi:10.1016/j.marpetgeo.2017.03.002

Mullins, H. T., Heath, K. C., Buren, H. M., and Newton, C. R. (1984). Anatomy of a Modern Open-Ocean Carbonate Slope: Northern Little Bahama Bank. *Sedimentology* 31, 141–168. doi:10.1111/j.1365-3091.1984.tb01956.x

Mutti, E., and Normark, W. R. (1991). "An Integrated Approach to the Study of Turbidite Systems," in *Seismic Facies and Sedimentary Processes of Submarine Fans and Turbidite Systems* (New York, NY: Springer), 75–106. doi:10.1007/978-1-4684-8276-8_4

Nagle, F., Stipp, J. J., and Fisher, D. E. (1976). K-ar Geochronology of the Limestone Caribbees and Martinique, Lesser Antilles, West Indies. *Earth Planet. Sci. Lett.* 29, 401–412. doi:10.1016/0012-821x(76)90145-x

Pamela Reid, R., Carey, S. N., and Ross, D. R. (1996). Late Quaternary Sedimentation in the Lesser Antilles Island Arc. *Geol. Soc. Am. Bull.* 108 (1), 78–100. doi:10.1130/0016-7606(1996)108<0078:LQSITL>2.3.CO;2

Paulatto, M., Laigle, M., Galve, A., Charvis, P., Sapin, M., Bayrakci, G., et al. (2017). Dehydration of Subducting Slow-Spread Oceanic Lithosphere in the Lesser Antilles. *Nat. Commun.* 8 (1), 1–11. doi:10.1038/ncomms15980

Payros, A., and Pujalte, V. (2008). Calciclastic Submarine Fans: An Integrated Overview. *Earth Sci. Rev.* 86, 203–246. doi:10.1016/j.earscirev.2007.09.001

Payton, C. E. (1977). Seismic Stratigraphy - Applications to Hydrocarbon Exploration. *Am. Assoc. Petroleum Geol.* 26, 1. doi:10.1306/M26490

Peters, S. E., and Loss, D. P. (2012). Storm and Fair-Weather Wave Base: A Relevant Distinction? *Geology* 40 (6), 511–514. doi:10.1130/g32791.1

Pichot, T., Patriat, M., Westbrook, G. K., Nalpas, T., Gutscher, M. A., Roest, W. R., et al. (2012). The Cenozoic Tectonostratigraphic Evolution of the Barracuda Ridge and Tiburon Rise, at the Western End of the North America-South America Plate Boundary Zone. *Mar. Geol.* 303-306, 154–171. doi:10.1016/j.margeo.2012.02.001

Pindell, J. L., and Barret, S. F. (1990). "The Caribbean Region, The Geology of North America,". *Geological Evolution of the Caribbean Region*, 339–374

Pindell, J. L., and Kennan, L. (2009). Tectonic Evolution of the Gulf of Mexico, Caribbean and Northern South America in the Mantle Reference Frame: an Update. *Geol. Soc. Lond. Spec. Publ.* 328 (1), 1–55. doi:10.1144/sp328.1

Polonia, A., Nelson, C. H., Romano, S., Vaiani, S. C., Colizza, E., Gasparotto, G., et al. (2017). A Depositional Model for Seismo-Turbidites in Confined Basins Based on Ionian Sea Deposits. *Mar. Geol.* 384, 177–198. doi:10.1016/j.margeo.2016.05.010

Posamentier, H. W., Erskine, R. D., and Mitchum, R. M., Jr. (1991). "Models for Submarine-Fan Deposition within a Sequence-Stratigraphic Framework," in *Seismic Facies and Sedimentary Processes of Submarine Fans and Turbidite Systems*. Editors P. Weimer and M. H. Link (New York: Springer), 127–136. doi:10.1007/978-1-4684-8276-8_6

Pratson, L. F., and Coakley, B. J. (1996). A Model for the Headward Erosion of Submarine Canyons Induced by Downslope-Eroding Sediment Flows. *Geol. Soc. Am. Bull.* 108 (2), 225–234. doi:10.1130/0016-7606(1996)108<0225:amfthe>2.3.co;2

Pratson, L. F., Ryan, W. B. F., Mountain, G. S., and Twichell, D. C. (1994). Submarine Canyon Initiation by Downslope-Eroding Sediment Flows: Evidence in Late Cenozoic Strata on the New Jersey Continental Slope. *Geol. Soc. Am. Bull.* 106 (3), 395–412. doi:10.1130/0016-7606(1994)106<0395:scibde>2.3.co;2

Principaud, M., Mulder, T., Gillet, H., and Borgomano, J. (2015). Large-scale Carbonate Submarine Mass-Wasting along the Northwestern Slope of the Great Bahama Bank (Bahamas): Morphology, Architecture, and Mechanisms. *Sediment. Geol.* 317, 27–42. doi:10.1016/j.sedgeo.2014.10.008

Puga-Bernabéu, Á., Webster, J. M., Beaman, R. J., and Guilbaud, V. (2011). Morphology and Controls on the Evolution of a Mixed Carbonate-Siliciclastic Submarine Canyon System, Great Barrier Reef Margin, North-Eastern Australia. *Mar. Geol.* 289 (1-4), 100–116. doi:10.1016/j.margeo.2011.09.013

Puga-Bernabéu, Á., Webster, J. M., Beaman, R. J., Reimer, P. J., and Renema, W. (2014). Filling the Gap: A 60 Ky Record of Mixed Carbonate-Siliciclastic Turbidite Deposition from the Great Barrier Reef. *Mar. Petroleum Geol.* 50, 40–50. doi:10.1016/j.marpetgeo.2013.11.009

Rankey, E. C., Riegl, B., and Steffen, K. (2006). Form, Function and Feedbacks in a Tidally Dominated Ooid Shoal, Bahamas. *Sedimentology* 53 (6), 1191–1210. doi:10.1111/j.1365-3091.2006.00807.x

Ratzov, G., Cattaneo, A., Babonneau, N., Déverchère, J., Yelles, K., Bracene, R., et al. (2015). Holocene Turbidites Record Earthquake Supercycles at a Slow-Rate Plate Boundary. *Geology* 43 (4), 331–334. doi:10.1130/g36170.1

Ratzov, G., Sosson, M., Collot, J.-Y., and Migeon, S. (2012). Late Quaternary Geomorphologic Evolution of Submarine Canyons as a Marker of Active Deformation on Convergent Margins: the Example of the South Colombian Margin. *Mar. Geol.* 315-318, 77–97. doi:10.1016/j.margeo.2012.05.005

Reijmer, J. J. G., Palmieri, P., and Groen, R. (2012). Compositional Variations in Calciturbidites and Calcidebrites in Response to Sea-Level Fluctuations (Exuma Sound, Bahamas). *Facies* 58 (4), 493–507. doi:10.1007/s10347-011-0291-z

Reijmer, J. J., Schlager, W., and Droxler, A. W. (1988). 15. Site 632: Pliocene-Pleistocene Sedimentation Cycles in a Bahamian Basin. *Proc. ocean Drill. program Bahamas Cover. Leg* 101, 626–636.

Richardson, P. L. (2005). Caribbean Current and Eddies as Observed by Surface Drifters. *Deep Sea Res. Part II Top. Stud. Oceanogr.* 52 (3-4), 429–463. doi:10.1016/j.dsr2.2004.11.001

San Pedro, L., Babonneau, N., Gutscher, M.-A., and Cattaneo, A. (2017). Origin and Chronology of the Augias Deposit in the Ionian Sea (Central Mediterranean Sea), Based on New Regional Sedimentological Data. *Mar. Geol.* 384, 199–213. doi:10.1016/j.margeo.2016.05.005

Saunders, M. A., Klotzbach, P. J., and Lea, A. S. R. (2017). Replicating Annual North Atlantic Hurricane Activity 1878-2012 from Environmental Variables. *J. Geophys. Res. Atmos.* 122, 6284–6297. doi:10.1002/2017JD026492

Schlager, W. (1989). "Drowning Unconformities on Carbonate Platforms," in *Controls on Carbonate Platform and Basin Development*. Editors P. D. Crevello, J. L. Wilson, J. F. Sarg, and J. F. Read (SEPM Special Publication), Vol. 44, 15–25. doi:10.2110/pec.89.44.0015

Schlager, W. (1998). "Exposure, Drowning and Sequence Boundaries on Carbonate Platforms," in *Reefs and Carbonate Platforms in the Pacific and Indian Oceans*. Editors G. F. Camoin and P. J. Davies (London: International Association of Sedimentologists/Blackwell), 3–21.

Schlager, W., Reijmer, J. J. G., and Droxler, A. (1994). Highstand Shedding of Carbonate Platforms. *Sepm Jsr* 64B (3b), 270–281. doi:10.1306/D4267FAA-2B26-11D7-8648000102C1865D

Seibert, C., Feuillet, N., Ratzov, G., Beck, C., and Cattaneo, A. (2020). Seafloor Morphology and Sediment Transfer in the Mixed Carbonate-Siliciclastic Environment of the Lesser Antilles Forearc along Barbuda to St. Lucia. *Mar. Geol.* 428, 106242. doi:10.1016/j.margeo.2020.106242

Shanmugam, G. (2016). Submarine Fans: A Critical Retrospective (1950-2015). *J. Palaeogeogr.* 5 (2), 110–184. doi:10.1016/j.jop.2015.08.011

SHOM (2018). MNT bathymétrique de façade de Saint-Martin et Saint-Barthélemy (Projet Homonim). Available at: https://geo.data.gouv.fr/fr/datasets/8302fdbac53efdc82fc83d06b24589623b8ec648. doi:10.17183/MNT_ANTN100m_HOMONIM_WGS84

Sola, F., Puga-Bernabéu, A., and Aguirre, J. (2017). Heterozoan Carbonate Deposition on a Steep Basement Escarpment (Late Miocene, Almería, South-East Spain). *Sedimentology* 64, 1107–1131. doi:10.1111/sed.12343

Spence, G. H., and Tucker, M. E. (1997). Genesis of Limestone Megabreccias and Their Significance in Carbonate Sequence Stratigraphic Models: a Review. *Sediment. Geol.* 112 (3-4), 163–193. doi:10.1016/s0037-0738(97)00036-5

Stanley, D. J. (1981). Unifites: Structureless Muds of Gravity-Flow Origin in Mediterranean Basins. *Geo-Marine Lett.* 1, 77–83.

Stein, S., Engeln, J. F., Wiens, D. A., Fujita, K., and Speed, R. C. (1982). Subduction Seismicity and Tectonics in the Lesser Antilles Arc. *J. Geophys. Res.* 87 (B10), 8642–8664. doi:10.1029/JB087iB10p08642

Stéphan, J. F., Mercier-de-Lepinay, B., Calais, E., Tardy, M., Beck, C., Carfantan, J. C., et al. (1990). Paleogeodynamic Maps of the Caribbean: 14 Steps from Lias to Present. *Bull. Soc. Geol. Fr.* 6 (8), 6–919.

Stow, D. A. V., and Mayall, M. (2000). Deep-water Sedimentary Systems: New Models for the 21st Century. *Mar. Petroleum Geol.* 17 (2), 125–135. doi:10.1016/s0264-8172(99)00064-1

Tcherepanov, E. N., Droxler, A. W., Lapointe, P., and Mohn, K. (2008). Carbonate Seismic Stratigraphy of the Gulf of Papua Mixed Depositional System: Neogene Stratigraphic Signature and Eustatic Control. *Basin Res.* 20 (2), 185–209. doi:10.1111/j.1365-2117.2008.00364.x

Tournadour, E., Mulder, T., Borgomano, J., Gillet, H., Chabaud, L., Ducassou, E., et al. (2017). Submarine Canyon Morphologies and Evolution in Modern Carbonate Settings: The Northern Slope of Little Bahama Bank, Bahamas. *Mar. Geol.* 391, 76–97. doi:10.1016/j.margeo.2017.07.014

Tournadour, E., Mulder, T., Borgomano, J., Hanquiez, V., Ducassou, E., and Gillet, H. (2015). Origin and Architecture of a Mass Transport Complex on the Northwest Slope of Little Bahama Bank (Bahamas): Relations between Off-Bank Transport, Bottom Current Sedimentation and Submarine Landslides. *Sediment. Geol.* 317, 9–26. doi:10.1016/j.sedgeo.2014.10.003

Vail, P. R., Audemard, F., Bowman, S. A., Eisner, P. N., and Perez- Cruz, G. (1991). "The Stratigraphic Signatures of Tectonics, Eustasy and Sedimentation-An Overview," in *Cyclic Stratigraphy*. Editors G. Einsele, W. Ricken, and A. Seilacher (New York: Springer), 617–659.

Weil-Accardo, J., Feuillet, N., Philibosian, B., Guihou, A., Jacques, E., Cabioch, G., et al. (2022). Interaction between Climate and Tectonics in the Northern Lesser Antilles Inferred from the Last Interglacial Shoreline on Barbuda Island. *Geochem. Geophys. Geosystems* 23, e2021GC010045. doi:10.1029/2021GC010045

Weimer, P., and Shipp, C. (2004). "Mass Transport Complex: Musing on Past Uses and Suggestions for Future Directions," in Paper presented at the Offshore Technology Conference, Houston, TX, May 2004 (OnePetro). doi:10.4043/16752-ms

Wilson, P. A., and Robert, H. H. (1995). Density Cascading: Off-Shelf Sediment Transport, Evidence and Implications, Bahama Banks. *Sepm Jsr* 65A, 45–56. doi:10.1306/D426801D-2B26-11D7-8648000102C1865D

Yose, L. A., and Heller, P. L. (1989). Sea-level Control of Mixed-Carbonate-Siliciclastic, Gravity-Flow Deposition: Lower Part of the Keeler Canyon Formation (Pennsylvanian), Southeastern California. *Geol. Soc. Am. Bull.* 101 (3), 427–439. doi:10.1130/0016-7606(1989)101<0427:slcomc>2.3.co;2

Conflict of Interest: The authors declare that the research was conducted in the absence of any commercial or financial relationships that could be construed as a potential conflict of interest.

Publisher's Note: All claims expressed in this article are solely those of the authors and do not necessarily represent those of their affiliated organizations, or those of the publisher, the editors, and the reviewers. Any product that may be evaluated in this article, or claim that may be made by its manufacturer, is not guaranteed or endorsed by the publisher.